FEDERAL UNIVERSITY OF CEARÁ

TECNOLOGY CENTER

CHEMICAL ENGINEERING DEPARTMENT

POS-GRADUATION PROGRAM IN CHEMICAL ENGINEERING

RESEARCH GROUP IN SEPARATIONS BY ADSORPTION - GPSA

PEDRO AUGUSTO SILVA DE MOURA

ASSESSING THE POTENTIAL OF ACTIVATED CARBONS FROM POLYETHYLENE TEREPHTHALATE (PET) AS ADSORBENTS TO SEPARATE CO_2 FROM FLUE GAS

FORTALEZA

2017

PEDRO AUGUSTO SILVA DE MOURA

ASSESSING THE POTENTIAL OF ACTIVATED CARBONS FROM POLYETHYLENE TEREPHTHALATE (PET) AS ADSORBENTS TO SEPARATE CO_2 FROM FLUE GAS

Dissertation submitted to Universidade Federal do Ceará as a requirement to obtain the Master's Degree in Chemical Engineering.

Supervisor: Profª. Diana Cristina Silva de Azevedo
Co-Supervisor: Dr. Enrique Vilarrasa Garcia

FORTALEZA

2017

Dados Internacionais de Catalogação na Publicação
Universidade Federal do Ceará
Biblioteca Universitária
Gerada automaticamente pelo módulo Catalog, mediante os dados fornecidos pelo(a) autor(a)

M889a Moura, Pedro Augusto Silva de.
Assessing the Potential of Activated Carbons from Polyethylene Terephthalate (PET) as Adsorbents to Separate CO2 from Flue Gas / Pedro Augusto Silva de Moura. – 2017.
65 f. : il. color.

Dissertação (mestrado) – Universidade Federal do Ceará, Centro de Tecnologia, Programa de Pós-Graduação em Engenharia Química, Fortaleza, 2017.
Orientação: Profa. Dra. Diana Cristina Silva de Azevedo.
Coorientação: Prof. Dr. Enrique Vilarrasa Garcia.

1. Adsorption. 2. Polyethylene Terephthalate - PET. 3. Carbon Dioxide - CO2. I. Título.
CDD 660

PEDRO AUGUSTO SILVA DE MOURA

ASSESSING THE POTENTIAL OF ACTIVATED CARBONS FROM POLYETHYLENE TEREPHTHALATE (PET) AS ADSORBENTS TO SEPARATE CO_2 FROM FLUE GAS

Dissertation submitted to Universidade Federal do Ceará as a requirement to obtain the Master's Degree in Chemical Engineering.

Supervisor: Prof[a]. Diana Cristina Silva de Azevedo
Co-Supervisor: Dr. Enrique Vilarrasa Garcia

Approved on 16 February 2017

Prof[a]. Diana Cristina Silva de Azevedo
Universidade Federal do Ceará

Dr[a]. Débora Aline Soares Maia
Universidade Federal do Ceará

Dr. Hugo Leonardo de Brito Buarque
Instituto Federal de Educação, Ciência e Tecnologia do Ceará

ACKNOWLEDGMENTS

First things first, I would like to thank God for everything.

To my mom's memory that is always beside me.

To my dad who takes care of me in many aspects of my life, all the time. My brother, Adroaldo, "*Brotherhood is to be the shadow of each other all the time*."

I would like to thank my entire family, especially my grandmother Francisca and grandfather Mourinha.

My supervisors, Profª. Diana and Dr. Enrique, for believing in my capacity, teaching and helping me in both my academic and personal life.

Friends and coworkers from the academy: Thalles, Rômulo, Davi, Débora, Alexandre, Isabela, Breno, Rafael, Edilson, Bruno, Melina, Karine, Santiago, Juliana, Suliene, Caiuã, Randreanne, Lairana, Rafaelle, Giovani, Felipe, Emmanuel, Rafael Siqueira, Zé Wilson, Dani, Rafael Morales, Bianca, Heather, Stuart, Ross, Greta, Charithea, Alícia, Raquel, Maria, Laura, Irma, Hilmar and Antonio that have made every day more pleasant throughout my master degree.

Just as importantly, friends outside the university, that have helped me on many occasions: Paula, Lívio, Felipe, Luciano, Volney, Rafael, Fabrício, Eduardo, Gilson, Allyson, CV, Duda, Vic, Haroldo, Felipe, Hélio Neto, Beto, Cezar, Ray, João Lucas, Mica, Pâmela, Sisi and many others.

Besides that, friendly professors: Moisés, Eurico, Célio, Parra, Conchi, Alírio, Mardônio, Luciana, Enrique and Rílvia from both within and outside my research group for many offerings of advice during my degree.

I would like to thank all people that have contributed directly or indirectly to this work.

Finally, I would like to thank as well the *Instituto Nacional del Carbon* – INCAR. Also, the Universidade de Campinas – UNICAMP. For last, not less important, *Coordenação de Aperfeiçoamento de Pessoal de Nível Superior – CAPES* and *Petróleo Brasileiro S.A. – Petrobras* for financial support.

“If you don't go after what you want, you'll never have it. If you don’t ask, the answer is always no. If you don't step forward, you're always in the same place.”

Nora Roberts

ABSTRACT

The Greenhouse Effect is a serious problem that concerns all countries and a solution to minimize or slow down this effect is mandatory. Increases in temperature and sea water level have caused some relevant impacts that can be felt by most of the world population. Carbon Dioxide (CO_2) is claimed as one of the main causes of this effect. Another problem in our society is the increasing production of Polyethylene Terephthalate (PET) polymers along the years, mainly used as soft drink bottles. Post-consumption bottles disposal is a huge problem to the world. The production of activated carbons from PET wastes generates materials with interesting properties for gas adsorption and storage. The aim of this work is to assess the potential of these activated carbons from PET (ACPXs) as adsorbents to separate CO_2 from flue gas. ACPXs have an exceptionally high surface area with pore sizes concentrated in a very narrow range (0.5-2 nm) and a hydrophobic surface with nearly no functional groups. Increasing burn-off degrees (22, 41 and 76%) led to adsorbents with a broader pore size distribution (PSD), but all mainly in the range of micropores. Single gas and mixed gas isotherms with CO_2 and N_2 reveal that the samples have an interesting selectivity for flue gas separation. These adsorbents have a high affinity for CO_2, ACPX-76 reaching an adsorption uptake of 6.323 mmol g^{-1} at 4 bar and 298 K. On the other hand, sample ACPX-22 has a higher narrow microporosity proportion (97.3%), which in turn gives a higher selectivity for CO_2 over N_2 (15.98 at 4 bar and 298 K). The differential adsorption enthalpy curves are typical of highly microporous samples reaching values close to those found in zeolites (40 kJ mol^{-1}) for low loadings, going down to values only slightly above the neat of condensation of CO_2 (17 kJ mol^{-1}) at higher loadings. It was found that the higher the burn-off, the wider the PSD and hence the greatest CO_2 capacity may be achieved. Nevertheless, higher CO_2/N_2 selectivities are found for the less activated sample, which has the lowest burn-off, lowest CO_2 uptake and the narrower Pore Size Distribution (PSD). The best trade-off of these parameters (working capacity, selectivity and adsorption enthalpy) was found for sample ACPX-41, with an intermediate burn-off, by comparison of an adsorbent performance indicator (API), as proposed in the literature.

Keywords: Adsorption . Polyethylene Terephthalate - PET . Carbon Dioxide - CO_2

RESUMO

O Efeito Estufa é um grave problema que preocupa todos os países, fazendo-se necessário encontrar uma solução definitiva para minimizar ou desacelerar seu efeito. O aumento da temperatura e do nível dos oceanos são alguns relevantes efeitos que podem ser sentidos por toda a população mundial. A concentração de Dióxido de Carbono (CO_2) no ar atmosférico é um dos principais responsáveis por este efeito. Outro grande problema em nossa sociedade, é a alta produção e acúmulo de resíduos de polímeros de Polietileno Tereftalato (PET) nos últimos anos, principalmente, como embalagens para produtos líquidos. A produção de carbonos ativados a partir do PET gera materiais com propriedades interessantes para a adsorção de gases e armazenamento. O objetivo central deste trabalho é avaliar o potencial destes carbonos ativados de PET (ACPX's) como adsorventes para a captura de CO_2 presente em diferentes correntes gasosas, como em gases de combustão. ACPX's tem altos volume de poro e área superficial com uma estreita distribuição de tamanho dos poros (0,5-2 nm) e uma superfície hidrofóbica, praticamente, sem grupos funcionais. Isotermas mono e multi componentes com CO_2 e N_2 revelaram uma seletividade interessante para um cenário de separação de gases de pós-combustão. Foram produzidos carbonos ativados em distintas condições de ativação, que levaram a distintos graus de "burn-off" (22, 41 e 76) e distribuição de tamanho de poros. Estes adsorventes têm uma elevada afinidade para o CO_2, ACPX-76 atinge a capacidade de adsorção de 6,323 mmol g^{-1} a 4 bar e 298 K. Por outro lado, a amostra ACPX-22 tem uma maior proporção de microporosidade estreita (97,3%), Por sua vez, uma maior seletividade para o CO_2 em relação a N_2 (15,98 a 4 bar e 298 K). A curva de entalpia de adsorção diferencial é típica de amostras altamente microporosas que atingem valores próximos aos encontrados em zeólitas (40 kJ mol^{-1}) para cargas baixas, descendo para valores apenas ligeiramente acima da pura condensação de CO_2 (17 kJ mol^{-1}) a cargas mais elevadas. Verificou-se que quanto maior a queima, maior a Distribuição do Tamanho de Poros (PSD) e, portanto, a maior capacidade de CO_2 pode ser alcançada. No entanto, maiores seletividades de CO_2 / N_2 são encontradas para a amostra menos ativada, que tem a menor queima, menor absorção de CO_2 e o PSD mais estreito. O melhor comprometimento desses parâmetros (capacidade de trabalho, seletividade e entalpia de adsorção) foi encontrado para a amostra ACPX-41, usando um indicador.

Palavras-Chave: Adsorção . Polietileno Tereftalato - PET . Dióxido de Carbono - CO_2

LIST OF FIGURES

LIST OF TABLES

ABREVIATIONS

NG	Natural Gas
GHG	Greenhouse Gases
GRF	Global Radiative Force
SV	Specific Volume
MSB	Magnetic Suspension Balance
PVOH	Polyvinyl Alcohol
PET	Polyethylene Terephthalate
MEA	Mono-ethanolamine
CCS	Carbon Capture and Storage
VSA	Pressure/ Vacuum Swing Adsorption
TSA	Temperature Swing Adsorption
PSA	Pressure Swing Adsorption
AC	Activated Carbon
TGA	Thermo-Gravimetric Analyzes
FT-IR	Fourier Transform Infrared Spectroscopy
TGA	Thermo-Gravimetric Analysis
PSD	Pore Size Distribution
2D NLDFT	2D Non-Local Density Functional Theory
QSDFT	Quenched Solid Density Functional Theory
DR	Dubinin-Radushkevich
LM	Langmuir Model
SM	Sips Model
BET	Brunauer-Emmett-Teller
ELM	Extended Langmuir Model
ESM	Extended Sips Model
MRELM	Multi-Region Extended Langmuir Model
IAST	Ideal Adsorbed Solution Theory
IUPAC	International Union of Pure and Applied Chemistry
MOF	Metal Organic Framework
API	Adsorbent Performance Indicator
WC	Working Capacity

SUMMARY

CHAPTER 1 – INTRODUCTION AND MOTIVATION

Life on earth may adjust to a temperature increase of 2 °C, approximately, but gas emissions have been rising steadily every year. Carbon Dioxide (CO_2) is claimed as one of the main causes of this effect (IPCC, 2014).

Several techniques have been developed to capture CO_2 from stationary emission points. Absorption, selective membrane permeation and cryogenic processes are some of them, but drawbacks, such as energy requirements, prevent their wide-spread use (THITAKAMOL; VEAWAB, 2009). Adsorption processes seem to be a promising alternative to reduce the CO_2 emission, due to low energy requirements and fast kinetics if a physisorbent with adequate capacity is found (RITTER, J.A., EBNER, 2009).

Another important environmental problem in the world is the amount of polyethylene terephthalate (PET) waste. The extensive use of this polymer in packages is due to its easy production and excellent water barrier properties, flexibility and thermal insulation. Oxygen permeability may be further reduced with an additional layer of polyvinyl alcohol (PVOH). Physical characteristics, such as transparency, semi-crystallinity, flexibility and high resistance to impact are excellent qualities for its use (BUNN, 1954).Present in several different products, particularly as soft drinks bottles and PET films, PET waste is nowadays a relevant environmental problem. Its consumption keeps rising and handling this material after consumption has become a major concern. Different solutions have been proposed for PET waste, such as recycling, incineration and disposal in landfills. Recycling is not enough to account for the generation of PET waste produced in the world. Incineration releases unwanted gases, such as CO_2, to the atmosphere. Disposal in landfills is the easiest and cheapest solution and has become the most common choice around the world. On other hand, this alternative has some disadvantages, such as atmospheric air pollution and contamination of underground aquifers.

The main objective of this work is to assess the potential of samples of activated carbons synthesized from PET wastes under different activation conditions to capture CO_2 considering different emission scenarios. Three samples were prepared from the same precursor (PET wastes) under different activation conditions. Nitrogen adsorption/desorption isotherms at 77 K, CO_2 adsorption isotherms at 273 K, infrared spectroscopy and thermo-gravimetric analysis experiments were performed to characterize morphology, surface chemical compositions and thermal stability of the obtained material. Working capacities, adsorption enthalpies and selectivity of CO_2 with respect to N_2 at 298, 323 and 348 K were measured in order to envisage its application in cyclic adsorption processes such as Pressure/Vacuum Swing adsorption (VSA) or Temperature Swing Adsorption (TSA).

CHAPTER 2 – LITERATURE REVIEW

2.1. ACTIVATED CARBONS FROM POLYETHYLENE TEREPHTHALATE (PET)

Dickson and Whinfield (USA) patented PET in 1941 (REX et al., 1961). Polyethylene Terephthalate (PET) is a crystalline thermoplastic polymer, which in natural state is a colorless resin. Crystal density is about 1.455 g cm^{-3}. The polymer has a high melting point (264 °C), due to rigid aromatic rings (**Figure 1**) (BUNN, 1954).

Figure 1. Polyethylene Terephthalate Monomer

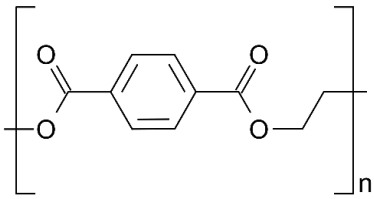

Source: (BUNN, 1954)

PET polymers production has increased along the years, mainly used as soft drinks bottles. Post-consumption bottles disposal is a huge problem to the world. The nearly exponential increase in world production of thermoplastics, polyurethanes, thermosets, elastomers, adhesives, coatings, sealants and PP-fibers along the last 60 years is illustrated in **Figure 2**. A friendly solution to the environment for the amount polymers already produced has to be done.

Figure 2. Production of plastic materials (thermoplastics and polyurethanes) and other plastics (thermosets, adhesives, coatings and sealants).

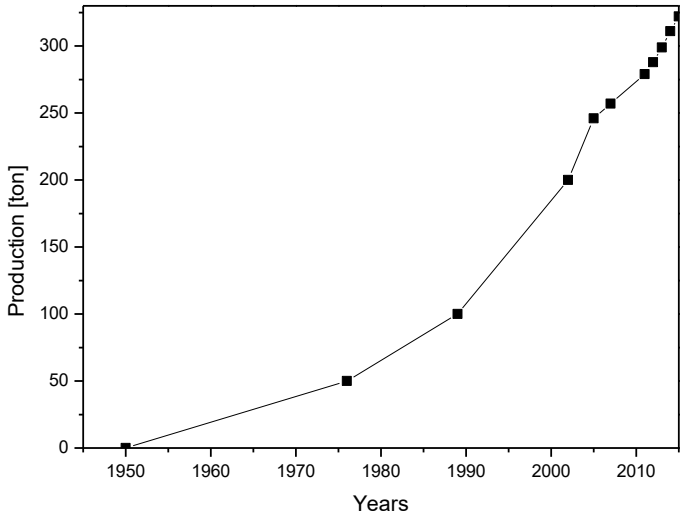

Source: Adapted (PLASTICSEUROPE, 2016)

Some of the solutions for plastics disposal in several countries are recycling and incineration. Using post-consumption soft-bottles as a substrate for activated carbon production through pyrolysis at around 1273 K is an interesting option, which has been addressed by some authors since 1997 (BLAZSÓ, 1997; PARRA et al., 2004b).

The production of activated carbons from PET generates materials with a high surface area and pore volume. The procedure involves four steps: (1) collection of similar materials with no impurities; (2) size reduction and sieving down to 0.5—1.0 mm particles; (3) pyrolysis at 1198 K under nitrogen atmosphere for 1 h to obtain the char; and (4) char activation with a carbon dioxide flow of 10 ml min^{-1} (PARRA et al., 2002, 2006, 2004a). By varying the activation time, samples of activated carbon with different textural properties may be obtained. The time of activation has a direct influence on the degree of burn-off (i.e. 720 min—2880 min), which in turn, affects the porosity. The pore size distributions (PSDs) obtained for different activation degree has been studied by (JAGIELLO et al., 2015) and is reproduced **Figure 3**. It is interesting to know how these different PSDs, within the micropore range, affect the working capacity, selectivity and adsorption enthalpy for a given gas separation or storage process.

Figure 3. Differential PSDs based on simultaneous fitting the 2D-HS models to both N_2 and CO_2 isotherms measured for the PC and its activated derivatives: PC-5, PC-23, PC-39, PC-63 and PC-85.

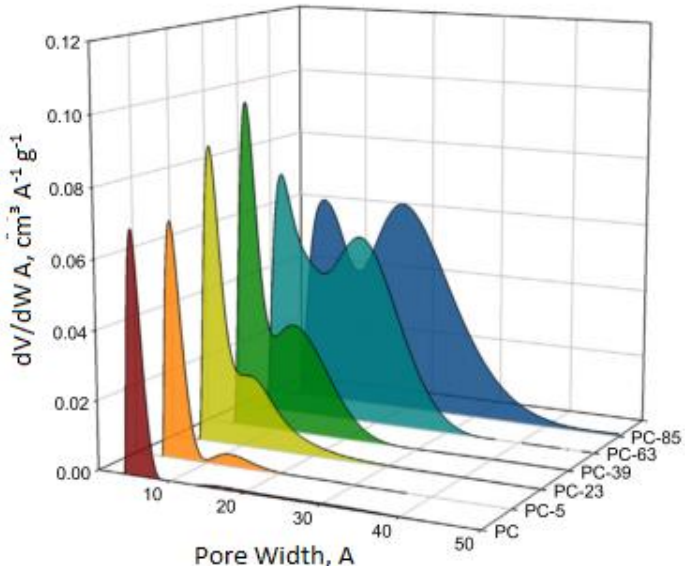

Source: Jagiello et al. 2015

2.2. GREENHOUSE EFFECT AND CO_2

The global warming is believed to be directly related to the high concentration of greenhouse gases (GHG) in the atmosphere (IPCC, 2014; KRUPA; KICKERT, 1989; SERREZE, 2010). The greenhouse effect is natural and necessary to maintain the earth temperature constant. In short, it is the retention of the sun heat by a thick layer of gases

on the earth surface. The problem is the intensification of this effect. Among all gases that contribute to global warming, three GHG deserve attention: carbon dioxide (CO_2), methane (CH_4) and nitrous oxide (N_2O). These gases are able to absorb and reissue infrared radiation (wavelength between 0.7 μm—100 μm) emitted by the sun. Apart from that, these gases have a high residence time in the atmosphere. (ESSENHIGH, 2009)

The main GHGs, their residence time in the atmosphere and their Global Radiative Forcing (GRF) are listed in **Table 1**. GRF refers to interference caused in equilibrium of temperature. Positive or negative coefficients mean warming or cooling the troposphere, respectively.

Table 1. Greenhouse Effect Gases (GEG)

Gases	**Residence Time [years]**	**GRF [Watts m^{-2}]**
CO_2	100	1.909
CH_4	10	0.500
N_2O	170	0.187

Source: (BUTLER, et al., 2015)

N_2O has the largest residence time, but a low GRF. CH_4 has an intermediate residence time and GRF, analyzing these parameters CH_4 was expected to have a moderate influence in global warming. In turn, CO_2 has a high reissue radiation and an intermediate residence time, so it is considered the most concerning GHG (ESSENHIGH, 2009; IPCC, 2014; KRUPA; KICKERT, 1989; SERREZE, 2010).

2.2.1. CARBON CAPTURE AND STORAGE (CCS)

Carbon Capture and Storage (CCS) processes are being developed aiming to capture CO_2 from its emission point, compress, transport and store it indefinitely. In several processes, the capture step accounts for around 75 % of the total cost (FIGUEROA et al., 2008). The most common CO_2 emission scenarios are natural gas pre and post combustion gas, in which cases, the other main competing gases are CH_4 and N_2, respectively (GARG; SHUKLA, 2009; PRAETORIUS; SCHUMACHER, 2009).

Adsorption is one of the capture technologies that may be used in CCS process. Besides, absorption, cryogenic distillation and membrane separations are other competing technologies (BAE et al., 2008).

Nowadays, absorption is a mature process in gas sweetening applied to natural gas and ammonia industries. Mono-ethanolamine (MEA) has widespread use in ammonia industry (chemicals, fertilizers and food), due to its high selectivity and reactive capacity. CO_2 from the extract may ordinarily reach 99.5 % purity and 98% recovery using MEA (KIM et al., 2013). On the other hand, amine absorption has some disadvantages, such as high-energy consumption, decreased equipment lifetime and frequent operational maintenance, mainly due to corrosion (THITAKAMOL; VEAWAB, 2009). Other

secondary problems are foam formation and amine degradation caused by sulfur dioxide (SO_2), nitrogen dioxide (NO_2), hydrochloric acid (HCl), hydrofluoric acid (HF) and oxygen (O_2).

Membranes made of carbon, polymers and inorganic components have also been studied for CO_2 separation from gas streams (KOROS; FLEMING, 1993; SANDRU; HAUKEBØ; HÄGG, 2010; SHEKHAWAT, 2003). Unlike absorption, a chemical as separation agent is not required and hence membranes have low maintenance cost (Ritter, J.A. and Ebner 2009). Their main disadvantages is fouling, particularly due to heavy hydrocarbons, causing sometimes irreversible damage (Ritter, J.A. and Ebner 2009; Sandru et al. 2010). Furthermore, they tend not to be efficient for high output pressures (YANG et al., 2008). Selective permeation in membranes is largely used to separate O_2, N_2 and CH_4, mainly when present in an atmosphere containing gases with larger diameters, as CO_2 and H_2S (SHEKHAWAT, 2003).

Cryogenic distillation separates gases with different vapor pressures at low temperatures. There is no need of chemical compounds, adsorbents or high pressure (DE STEFANI; BABA-AHMED; RICHON, 2003; TUINIER et al., 2010). However, there is a high energy consumption, pipes tend to clog with solidification of CO_2 and heat loses may be a problem (TUINIER et al., 2010).

If compared to these technologies, gas adsorption potentially requires less energy input. The adsorbent may be reused in cycles upon changes in pressure (VSA), temperature (TSA) or concentration (Concentration Swing Adsorption – CSA) (WONG; BIOLETTI, 2002).

2.2.2. FLUE GASES AND CO_2

CO_2 emissions linked to energy generation by fuel combustion may be found in three different scenarios: pre-combustion, oxy-combustion and post-combustion. Schematically the three emission scenarios are shown in **Figure 4**. Post-Combustion is the most commonly found scenario in thermo-electric energy generation. Fuels are burned with atmospheric air and N_2 and CO_2 are the major effluent gases (flue gas), besides water vapor (KANNICHE et al., 2010). Pre-Combustion involves gasifying the fuel to synthesis gas (CO_2 + H_2) prior to hydrogen combustion and energy conversion. The combustion effluent is only water, which is a clear advantage. However, this requires changing the energy vector from carbon to hydrogen. Oxy-Combustion consists in burning fuels with pure O_2 so that the combustion products are only water vapor and CO_2, which may be readily separated by condensation. However, in the absence of nitrogen, combustion temperature would be extremely high and current thermo-electric plant equipment would not withstand such conditions.

The most common emission scenario in current power plants are flue gases (post combustion), which poses challenges for CO_2 capture. It is found in low concentration (5-15% vol.), low pressures and relatively high temperatures. All of these are very weak driving forces for separation, irrespective the chosen technology.

Figure 4. Combustion Flue Gas Scenarios

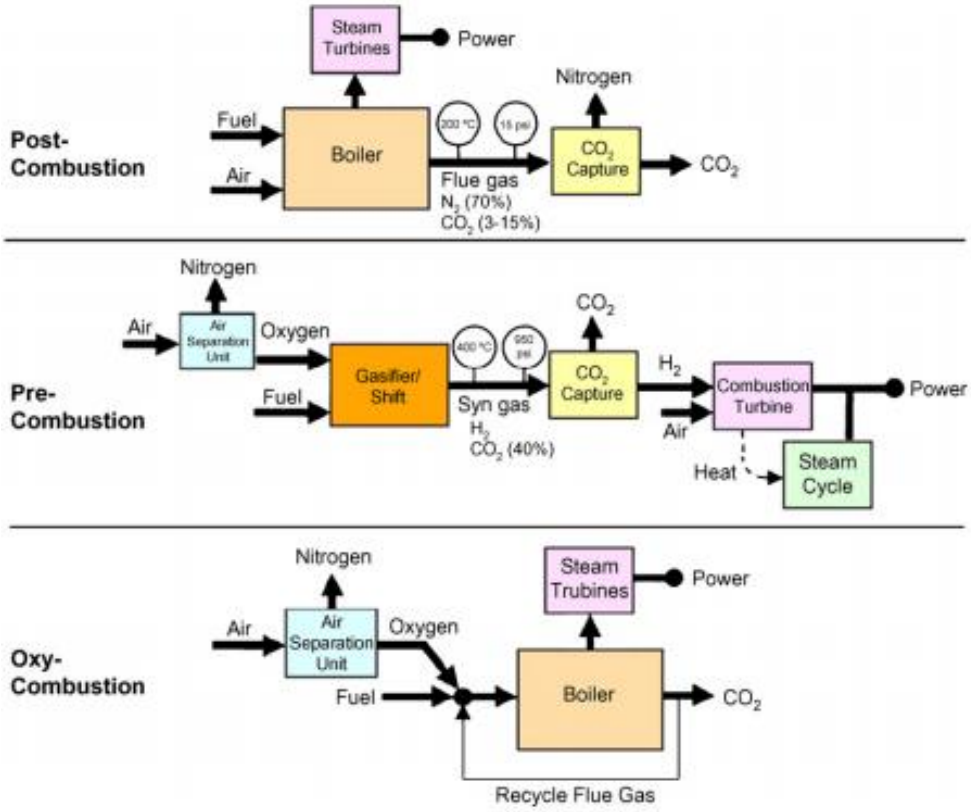

Source:(VASEGHI; AMIRI; PESARAN, 2012)

2.3. ADSORPTION

One of the most common application of adsorption in everyday life is odor removal inside refrigerators by volatile compounds released by food decomposition.The compounds responsible for odor "adhere" to the char surface at low temperatures. Adsorption is hence defined as the spontaneous concentration of molecules from a fluid at the vicinity of an interface (**Figure 5**), usually between a solid and a fluid, due to unbalanced forces at the surface. This definition is restricted to physisorption, which is an exothermic and reversible process. The free fluid that is named the adsorptive, the molecules concentrated on the surface is the adsorbate and the adsorbent is the solid surface. Desorption is the opposite process of molecules concentration in adsorbent surface.

Figure 5. Adsorption Process

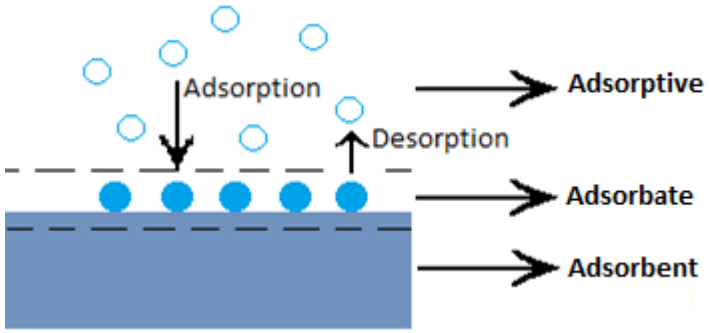

Adsorption can be classified in two types: physisorption and chemisorption. Physisorption or physical adsorption involves weak interactions between adsorbate and adsorbent, such as electrostatic interactions and van der Waals forces. Chemisorption or chemical adsorption, on the other hand, is characterized by strong interactions between adsorbate and adsorbent, such as covalent bonding, heats of adsorption being in the order of magnitude of that of chemical reactions. Some other characteristics are summarized in **Table 2** (SING; ROUQUEROL; ROUQUEROL, 2014).

Table 2. Comparison between Physical and Chemical Adsorption

Characteristic	**Physical Adsorption**	**Chemical Adsorption**
Adsorption Enthalpy	1 - 15 kcal mol^{-1}	9.5 - 95 kcal mol^{-1}
Adsorbate-adsorbent Interactions	Van Der Waals Bonds; Electrostatic Bonds	Covalent Bonds
Temperatures	Low Temperatures	Wide range of Temperatures
Number of adsorbed Layers	Mono and Multi	Mono
Kinetics	Fast and Reversible	Slow and Irreversible

Source: (Ruthven, 1984).

2.3.1. ADSORPTION ISOTHERMS

Adsorption equilibrium data is represented by isotherms or isobars, which describe adsorbed phase concentration (g or mol per unit mass adsorbent) as a function of temperature and pressure. Brunauer, Deming and Teller proposed the BDDT classification with five types of isotherms (BRUNAUER et al., 1940). Later, a sixth category was identified (SING et al., 1985). The International Union of Pure and Applied Chemistry (IUPAC) has recently defined six isotherms categories (THOMMES et al., 2015), which are shown in **Figure 6**.

In **Figure 6**, types Ia and Ib are reversible and concave with respect to the relative pressure axis. There is a steep increase of adsorbed mass at low pressures followed by a constant plateau.Type I isotherms are typical of solids with pore sizes majorily located in the micropore range (up to 2 nm). Type Ia isotherms have narrow micropores and Ib isotherms have wide micropores. Type II isotherms are also reversible with no hysteresis. They are concave at low relative pressure, then reach a plateau and finally become convex at high relative pressures. Nonporous or macroporous solids have this type of isotherm. Type III isotherms are convex relative to the pressure axis over the whole pressure range. Interactions between the adsorbent and adsorbate are much weaker than those between the adsorbent molecules. Non-porous or macroporous materials commonly exhibit this kind of isotherms. Type IVa isotherms are much more common than Type IVb. They are normally observed in materials with a large pore size distribution, particularly in mesopore size range. Hysteresis is commonly find in type IV isotherms and it is due to capillary condensation inside pores. Type V isotherms are convex at low relative pressures, like type III. Nevertheless, there is hysteresis, usually caused by pore filling

and emptying in mesopores. Type VI isotherms is associated with layer-by-layer adsorption in very homogeneous materials. It is a relatively rare isotherm.

Figure 6. Classification of vapor adsorption isotherms combining proposal from IUPAC, linking the relative pressure and adsorbed mass.

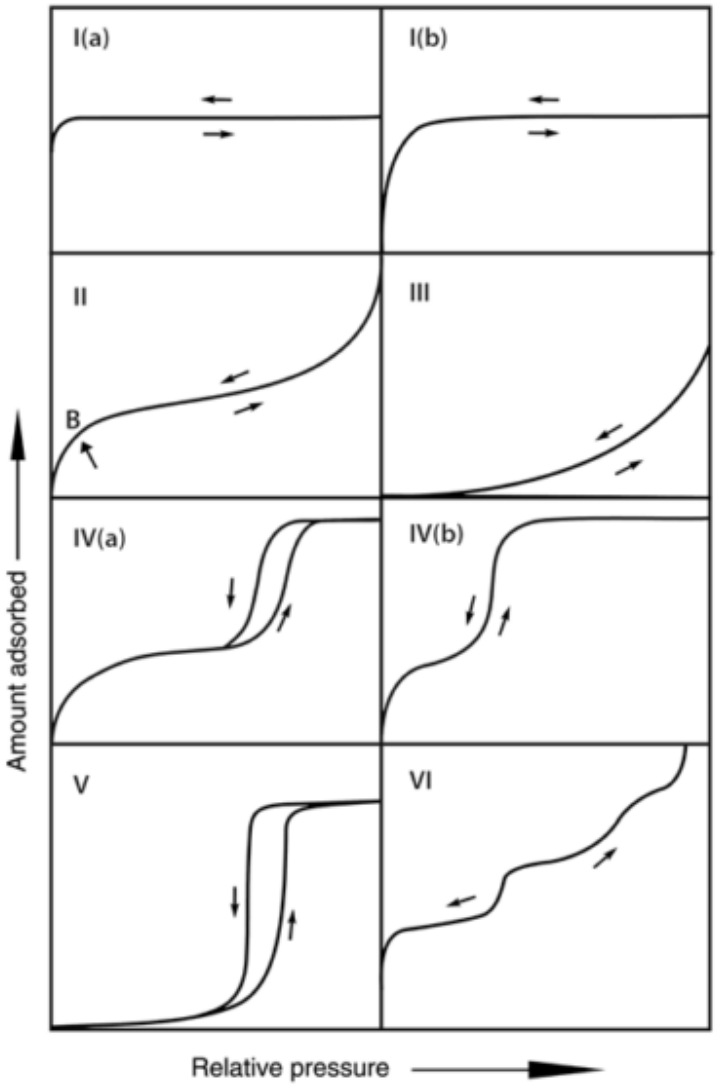

Source: (THOMMES et al., 2015)

Convenient application of equilibrium models to the adsorption isotherms of probe gases (such as N2 at 77K) allows for the determination of important textural features of the adsorbent, such as pore volume, specific surface area, PSD and average pore size. With respect to pore sizes, solids are also classified in three types according to IUPAC:

- Micropores: pore sizes below 2 nm;
- Mesopores: pore sizes between 2 nm and 50 nm;
- Macropores: pore sizes above 50 nm.

2.3.2. ADSORBENTS AND ACTIVATED CARBONS

Adsorbents for gas separation or storage/delivery by physisorption must have a number of desirable features:

- Predominantly microporous, because gas molecules are small and only sufficiently narrow pores would provide potential for significant adsorption;
- High surface area, to allow for high adsorption capacity and hence more compact adsorbers;
- Nearly hydrophobic surface, so that the main retention mechanism are weak van der Waals forces. This allows for reversible fast adsorbent regeneration with low energy requirements;
- Good mechanical resistance and suitable particle (grain) size to avoid high pressure drops in adsorption columns;
- Good selectivity of the target adsorbate with respect to other gases, in the case of separation/purification.

All of these characteristics may potentially be found in activated carbons, depending on their starting material and activation mode. Activated Carbons (AC) have an amorphous structure, which is generally accepted to be composed of randomly packed graphene sheets, which generate a network of slit-like pores. It can be produced from several raw materials, such as coconut shells, anthracite, peach/olive stones and wood (ALBANEZ, 2008). In Brazil, bituminous carbon, wood and coconut shells are the most widely used precursos (DI BERNARDO, 2005). The annual production is about 1,437 million tons in 2014 (MARKET, 2017) in different industrial applications, e.g. adsorbent, catalyst or catalyst support for gas and liquid (KIM; KANG, 2008). Pyrolysis is the most common method to prepare these adsorbents at temperatures lower than 1273 K. In this process most of non-carbon elements are volatilized, e.g. oxygen, nitrogen and sulfur compounds. After that, a physical or chemical activation procedure is used to increase the adsorption capacity. The activation procedure involves particle size, chemical agents and method of mixing to obtain a specific activated carbon. Several activated carbon sources are shown in **Table 3**.

Table 3. Activated Carbons Studies

Precursor	**Purpose**	**Reference**
Palm Shell	CO_2 Adsorption	(KACEM; PELLERANO; DELEBARRE, 2015)
Olive Stones	Synthesis Material	(SILVESTRE-ALBERO et al., 2012)
Phenol-formaldehyde resin	CO_2 Adsorption	(GARCIA et al., 2013)
PET polymers	Hydrogen Storage	(PARRA et al., 2004a)
PET polymers	Synthesis Material	(PARRA et al., 2002)

2.3.3. ENTHALPY OF ADSORPTION

Adsorption calorimetry is a thermodynamic technique that allows the direct measurement of the total heat released during the adsorption process (WADSÖ, 1997). Overall, calorimetry is a tool of high accuracy and precision to characterize adsorbents and surface phenomena. One of the drawbacks of this widespread technique is the need to develop tailor-made equipment for a given phenomenon (reaction, dissolution, adsorption, etc.). One must also take into account that the adsorption energy measured by these devices is the sum of the fluid-fluid and fluid-solid interactions.

Physisorption is exothermic with heat transfer from the adsorbed phase to the surrounding fluid. Thermal effects are important to predict and to handle bed heating and cooling upon adsorption and desorption cycles, respectively. By measuring the evolved adsorption heat as a function of the adsorbed phase concentration, one can also investigate the heterogeneities of the solid surface (DUNNE et al., 1996; ROUQUEROL et al., 2014). A decrease in the differential heat of adsorption as the adsorbed phase concentration increases is common for heterogeneous solid, whereas a constant adsorption enthalpy for increasing adsorbed phase concentration is characteristic of homogeneous surfaces (LLEWELLYN, 2000). These heat curves may be measured directly, with the aid of a micro-calorimeter, or indirectly from equilibrium adsorption data measured at various temperatures, the so-called isosteric enthalpy of adsorption.

The isosteric enthalpy of adsorption (ΔH) may be calculated from Clausius-Clapeyron Equation (**Equation 2.1**). By plotting $\ln(P)$ versus $\frac{1}{T}$, the slope gives $\Delta H/R$.

$$\Delta H_{ads} = -R \cdot \left(\frac{\partial \ln(P)}{\partial (1/T)} \right)_q \qquad (2.1)$$

2.3.4. ADSORPTION EQUILIBRIUM MODELS

Several models have been proposed to describe mono and multi component gas adsorption behavior, which some are summarized in **Table 4** and **Table 5**, respectively.

Table 4. Mono Component Adsorption Isotherm Models

Isotherm Model	Equation	
Henry or Linear	$q_{eq} = H \cdot P$	(2.2)
Langmuir (LM)	$q_{eq} = \frac{q_{máx} \cdot b \cdot P}{1 + b \cdot P}$	(2.3)
Sips (SM)	$n_{eq} = \frac{n_{max}^{\infty} \cdot (K \cdot P)^{C}}{1 + (K \cdot P)^{C}}$	(2.4)
Freundlich	$q_{eq} = K_{eq} \cdot P^{1/m}$	(2.5)
Toth	$q_{eq} = \frac{q_{máx} \cdot K \cdot P}{(1 + (K \cdot P)^{t})^{1/t}}$	(2.6)
Brunauer-Emmett – Teller (BET)	$n = \frac{\left(\frac{P}{P_{\circ}}\right)}{\left[\frac{1}{n_m C} + \left(\frac{C-1}{n_m C}\right)\left(\frac{P}{P_{\circ}}\right)\right] \cdot \left[1 - \left(\frac{P}{P_{\circ}}\right)\right]}$	(2.7)

Table 5. Multi Component Adsorption Isotherm Models

Isotherm Model	Equation	
Extended Langmuir (ELM)	$q_{eq_i} = \frac{q_{máx_i} \cdot b_i \cdot P_i}{1 + b_i \cdot P_i + b_j \cdot P_j}$	(2.8)
Extended Sips (ESM)	$n_{eq_i} = \frac{n_{max_i}^{\infty} \cdot (K_i \cdot P_i)^{C_i}}{1 + (K_i \cdot P_i)^{C_i} + \left(K_j \cdot P_j\right)^{C_j}}$	(2.9)
Multi-Region Extended Langmuir (MRELM)	$q_{eq_i} = \frac{q_{máx_j} \cdot b_i \cdot P_i}{1 + b_i \cdot P_i + b_j \cdot P_j} + \frac{(q_{máx_i} - q_{máx_j}) \cdot b_i \cdot P_i}{1 + b_i \cdot P_i}$ $q_{eq_j} = \frac{q_{máx_j} \cdot b_j \cdot P_j}{1 + b_i \cdot P_i + b_j \cdot P_i}$	(2.10)
Ideal Adsorbed Solution Theory (IAST)	$\pi_i^{*} = q_{m_i} \cdot \ln(1 + b_i \cdot P)$	(2.11)

Some models have thermodynamic inconsistencies. For instance, in Toth and Freundlich models, when pressure tends to zero, the isotherm equation does not reduce to Henry's Law (**Equation 2.13**) (TÓTH, 2003).

$$\log_{P \to 0} q/P = constant \tag{2.12}$$

The LM (**Equation 2.3**) considers a homogeneous adsorbent surface, meaning that all adsorption sites have the same energy. Besides, each site will only host one gas molecule and there is no interaction between the gas molecules already adsorbed. This model usually fits well experimental data for microporous materials (LANGMUIR, 1918), although none of the underlying hypotheses holds in practice. Nevertheless, it provides a two-parameter robust equation that is able to predict adsorption equilibria in many cases. In practice, parameter (q_{max}) refers to the maximum quantity adsorbed in all

adsorption sites; and (b) expresses the magnitude of the interaction between adsorbate and adsorbent.

The SM (**Equation 2.4**) is an extension of LM. It includes an additional parameter 'C', which accounts for the heterogeneity of the adsorbent surface (MYERS; PRAUSNITZ, 1965). Hence, this equation includes three parameters: parameters related to maximum adsorbed quantity (n_{max}^{∞}); interaction between adsorbed particles (K) and heterogeneous sample surface (C) that is a characteristic of a given adsorbent.

The Freundlich Model (**Equation 2.5**) is the most empirical model attempting to describe adsorption on a heterogeneous adsorbent surface. The parameter (m) qualifies the adsorbent heterogeneity and commonly admits values higher than unity. Toth Model (**Equation 2.6**) is an empiric model that can be applied for a wide pressure range. The (t) parameter accounts for the heterogeneity of the sites (TÓTH, 2002).

The BET Model (**Equation 2.7**) (BRUNAUER et al., 1940) also assumes an energetically homogeneous surface, but take into account the formation of multiple adsorbed layers. The first adsorbed molecules helps the formation of a second layer, providing an adsorption site and so forth. From the second and subsequent layers, the adsorbed molecules behave as a saturated liquid. The parameter (n) represents the equilibrium absorbed concentration; (n_m) is the adsorbed concentration in a monolayer; (C) is exponentially related to E_1 (the first-layer adsorption); ($P/P_\circ$) is the relative pressure.

The ELM (**Equation 2.8**), follows a similar concept as LM, but applied to multicomponent adsorption. All parameters (b_i, b_i, q_{max_i}, q_{max_j}) are those measured from single component isotherms. Extended Sips Model (**Equation 2.9**) is analogous to its version for mono-component model. Both ELM and ESM are based on the adsorbed concentration of each component of a mixture as a function of the partial pressures of all components present at a given temperature. They are, normally used in binary atmosphere with CO_2, CH_4 and N_2, due to their reasonable accuracy and simplicity. Nevertheless, their accuracy in the prediction of multicomponent adsorption relies heavily on good measurements of single-component isotherms.

The Multi-Region Extended Langmuir (**Equation 2.10**) is a model that has the main difference in the existence of two different pores in the material surface. One of them, adsorb both adsorbates, but the other adsorbent site only adsorb the most affinity adsorbate. Other important fact is the presence of $q_{máx_j}$in amount adsorbed of i and j estimation, due to a majority physisorption, so the sites into the material are almost the same, which in turn causes the same maximum adsorbed in both adsorbates (VILARRASA-GARCÍA et al., 2015). IAST (MYERS; PRAUSNITZ, 1965) (**Equation 2.11**) is used to predict multi-components isotherms, using parameters from mono-components isotherms. In opposition to the other models, an analytical solution is not possible for IAST. This model has a high dependence for spreading pressure and adsorbed mass estimations at low pressures (MYERS; PRAUSNITZ, 1965).

To estimate the accuracy of each adsorption model, a deviation function based on the difference of the experimental and calculated amount adsorbed (**Equation 2.13**).

$$D(\%) = \frac{1}{N}\sum_{i=1}^{N_t}\frac{(q_{i,est} - q_{i,exp})^2}{q_{i,exp}} \cdot 100 \quad (2.13)$$

2.3.5. EXCESS AND ABSOLUTE MASS

The definition for excess mass is all mass variation obtaining in the sample due to the adsorption. The adsorbate not adsorbed in the pores, just compressed into it, do not count for mass variations, so it is not measured. The devices normally only measure the excess mass, so some calculations are necessary. The absolute mass considers the adsorbates, not just adsorbed, but also compressed into the pores.

It is useful distinguish between excess and absolute adsorbed concentrations. Absolute adsorbed concentration is the total amount of sorbate (per unit mass adsorbent) contained in the adsorbed phase volume. Excess adsorbed concentrations is the amount of sorbate (per unit mass adsorbent) that exceeds the concentration to be excepted for a free fluid in given conditions of temperature and pressure. Because it is practically impossible to define the exact volume of the adsorbed phase, it is excess adsorbed concentration, which is actually measured in experimental devices. Additionally, in a gravimetric device, mass variations of an adsorbent are also subject to buoyancy forces acting on the solid and other suspended parts of the equipment. Therefore, excess adsorption (m_{exc}) may be measured from mass variations (Δm) measured according to **Equation 2.14** (DREISBACH; STAUDT; KELLER, 1999), where the second term on the right-hand side of the equation accounts for the buoyancy effects.

$$\Delta m = m_{exc} - \rho_g(V_B + V_s) \quad (2.14)$$

Where (Δm) is the mass variation per unit mass adsorbent (m_{exc}) is the excess adsorbed concentration; (ρ_g) is gas phase density, (V_B) is the volume of suspended parts inside the measuring chamber and (V_s) is the adsorbent solid volume. In order to estimate the absolute adsorbed concentration, the amount of compressed gas present in the adsorbed phase volume should be added to the excess adsorbed concentration as in (**Equation 2.15**) (MURATA; KANEKO, 2001).

$$q_{abs} = m_{exc} + \frac{\rho_g \cdot V_{ads}}{m_s \cdot MM} \quad (2.15)$$

In **Equation 2.15**, (q_{abs}) is the absolute adsorbed concentration; (m_{exc}) is the excess adsorbed concentration; (ρ_g) is gas phase density, (V_{ads}) is the adsorbed phase volume; (m_s) is the adsorbent solid mass and (MM) is the gas molar mass. All variables can be measured, calculated or found in the literature, except V_{ads}, which has to be

estimated, according to some sound assumptions. For microporous adsorbents, it may be assumed the adsorbed phase volume is the specific pore volume (**Equation 2.16**) (QUIRKE; TENNISON, 1996).

$$V_{ads} = V_P \tag{2.16}$$

2.3.6. SURFACE AREA AND PORE VOLUME

SURFACE AREA

In order to calculate the specific surface area from adsorption/desorption isotherms of probe molecules at their saturation temperature (e.g., N_2 at 77K), the BET Model (**Equation 2.7**) is commonly applied. The superficial area estimation comes from the total molecules adsorbed in the monolayer. The model equation is generally rearranged as in (**Equation 2.17**). By plotting $\frac{\left(\frac{P}{P_\circ}\right)}{n\left[1-\left(\frac{P}{P_\circ}\right)\right]}$ vs. $\left(\frac{P}{P_\circ}\right)$ in a sufficiently low pressure range, a straight line is to be expected. The slope $\left(\frac{C-1}{n_m C}\right)$ and the intercept is $\left(\frac{1}{n_m C}\right)$. The BET method can be applied in a pressure range of relative pressure from 0.05 to 0.35. Since n_m is the number of mols to cover a monolayer, if the cross section of the probe molecule is known (σ), it is possible to estimate the surface area (A_{BET}) using **Equation 2.18** (SING et al., 2014), where Avogadro Number (*AN)* ($6.023 \cdot 10^{23}\ mol^{-1}$).

$$\frac{\left(\frac{P}{P_\circ}\right)}{n\left[1-\left(\frac{P}{P_\circ}\right)\right]} = \frac{1}{n_m C} + \left(\frac{C-1}{n_m C}\right)\left(\frac{P}{P_\circ}\right) \tag{2.17}$$

$$A_{BET} = n_m \cdot \sigma \cdot AN \tag{2.18}$$

TOTAL PORE VOLUME

The total pore volume is estimated using **Equation 2.19**, where (n_{N_2}) is the adsorbed concentration at a relative pressure $\left(\frac{P}{P_\circ}\right)$ equal 0,99. At this relative pressure is assumed that all pores are filled with liquid adsorbate (THOMMES et al., 2015). In **Equation 2.19**, (*MM*) is the molar mass of N_2 and (ρ_{N_2}) is the density of liquid N_2.

$$V_P = n_{N_2} \cdot \frac{MM_{N_2}}{\rho_{N_2}} \tag{2.19}$$

MICROPORE VOLUME

The micropore volume is the pores whose diameters are in the range of 0.5 < d < 2.0 nm. It can be defined by the volume found from Dubinin-Stoeckli method (DS) (DUBININ; STOECKLI, 1980) that is similar to Dubinin-Radushkevich considering a surface of different pores structures. (**Equation 2.20**), where *W* is the total pore volume and *B* is the structural constant.

$$W = \int_0^{\infty} f(B) \cdot \exp\{-By\}\, dB \tag{2.20}$$

PORE SIZE DISTRIBUTION (PSD)

The PSD is one of the main properties of a physisorbent intended for gas separation/purification and storage. Besides that, ideal PSD obtained from theoretical calculations are useful in developing new adsorbents. N_2 isotherms at 77 K are usually used to extract the PSD, although at this temperature, N_2 molecules tend to diffuse slowly and equilibrium may not be reached in reasonable time for ultramicropores. In order to overcome this problem, CO_2 isotherms at 273 K are commonly used to assess the narrow micropores (RODRIGUEZ-REINOSO, F., LINARES-SOLANO, 1988)

The PSD can be estimated using methods as 2D Non-Local Density Functional Theory (2D NL-DFT) (JAGIELLO et al., 2015). The 2D NLDFT considers the fluid structure close to narrow micropores and mesopores. In addition, it quantifies the adsorption from intermolecular potentials of interactions between fluid-fluid and solid-fluid. From **Equation 2.21**, it is related the theoretical microscopic adsorption and the experimental adsorption isotherm.

$$I_{\left(\frac{P}{P_o}\right)} = \int_{w_{min}}^{w_{max}} I\left(\frac{P}{P_o}, w\right) f(w) dw \tag{2.21}$$

Where, $I_{\left(\frac{P}{P_o}\right)}$ is the experimental adsorption isotherm, w is the pore size and , *f(w)* is the pore size distribution. The 2D NLDFT consists in the total integration of that function (*f(w)*) in the material.

2.3.7. SELECTIVITY

The selectivity is an important characteristic of an adsorbent in gas separations. It quantifies the adsorbent preference to adsorb a gas instead of another. This parameter can be defined by different ways. The capacity to adsorb CO_2 preferentially to N_2 is important for industrial applications from mono-components isotherms the selectivity is defined as the division between masses. From binary isotherms, the selectivity is defined using the binary model that better adjust the isotherms, calculated using **Equation 2.22**.

$$Sel_{CO2/N2} = \frac{q_{CO2}}{q_{N2}} \cdot \frac{P_{N2}}{P_{CO2}} \tag{2.22}$$

2.3.8. WORKING CAPACITY

The working capacity (WC) is defined as the difference between the adsorption capacities at two specific working pressures. It is important to be considered in cyclic processes based on pressure swings to regenerate and reuse the adsorbent. For instance, if one assumes that the adsorption step is carried out at 4 bar and the dessorption step at 1 bar, the working capacity is calculated as **Equation 2.23**.

$$WC(1-4\ bar) = \left[q_{eq}\right]_{4bar} - \left[q_{eq}\right]_{1bar} \tag{2.23}$$

2.3.9. ADSORBENT PERFORMANCE INDICATOR – API

In order to compare adsorbents indicated for a given gas separation/ purification, a performance indicator has been suggested in the literature (WIERSUM et al., 2013) (**Equation 2.24**).

$$API = \frac{(\alpha_{i,j} - 1)^a \cdot {WC_i}^b}{{\Delta H^c}_i} \tag{2.24}$$

Where *a*, *b* and *c* are empirical parameters, which may be turned according to the desired separation/ purification process. α is the selectivity *i* with respect to *j*; *WC* is the working capacity of the most adsorbed component (*i*); and ΔH is the adsorption enthalpy of the most adsorbed component (*i*).

CHAPTER 3 – EXPERIMENTAL

3.1. MATERIALS

3.1.1. GASES

Three different gases were used, two of them were adsorbates and helium (He) line was used for calibration procedures. They were supplied by White Martins Praxair Inc. (Brazil) under the purities shown in **Table 6**.

Table 6. Gases used in experiments

Gas	Chemical Formula	Purity	Molar Mass [g mol^{-1}]	Characteristics
Helium	He	99.999	4.00	Inert and Non-flammable
Nitrogen	N_2	99.999	28.01	Non- flammable and Non- Toxic
Carbon Dioxide	CO_2	99.800	44.01	Non- flammable and Toxic

3.1.2. ADSORBENTS

All experiments were carried out with activated carbons samples obtained from polyethylene terephthalate. Activated carbons obtained using the procedure according to that described in the literature (PARRA et al., 2002, 2004a). They were labeled as ACPX-22, ACPX-41 and ACPX-76, according to the key given in **Table 7**. Briefly, all the activated carbon samples by the pyrolysis of PET at 998.15 K for 2 hours under nitrogen atmosphere so as to form char. Then, the char was activated under CO_2 flow (10 mL min^{-1} for an average char mass of 5 g) at 1198 K for 24 h, 36 h and 72 h, respectively.

The burn0off degree is calculated using the mass variation at activation process (**Equation 3.1**).

$$BO = \frac{M_{BACO2} - M_{AACO2}}{M_{BACO2}} \tag{3.1}$$

Thus, three adsorbents were produced: ACPX-22, ACPX-41 and ACPX-76.

Table 7. Obtained ACPX Samples

Samples Code	Meaning
AC	Activated Carbon
P	Polyethylene Terephthalate
X	Diameter (500 µm < d < 1000 µm)
00	Burn-off degree

3.2. METHODS

3.2.1. ADSORBENTS CHARACTERIZATION

All ACPX samples were characterized regarding their thermal degradation properties, surface functional groups and textural features.

Thermo-Gravimetric Analyses (TGA) were performed in a TGA/DTA Setaram Instrumental Setsys 16/18 model, coupled to a mass spectrometer, ThermoStar, by Pfeiffer, model. The experiments were carried out under nitrogen flux (16 mL min^{-1}) and in the range of room temperature (298 K) to 1273 K at a heating rate of 10 K min^{-1} to obtain the regeneration temperature. Approximately 10 mg sample was loaded in a sample port made of alumina. Textural characteristics of the sample were obtained from N_2 and CO_2 adsorption/desorption isotherms at 77 K and 273 K, respectively using ASAP 2020 and TriStar models, Micromeritics Instrumental, U.S.A, respectively. Prior to N_2 adsorption, the sample was degassed at 423 K and (10^{-3} - 10^{-4} mbar) for 5 hours. Fourier Transform Infrared Spectroscopy (FT-IR) was performed in a Nicolet 6700 FTIR Thermo Scientific Spectrophotometer (128 scans with resolution of 4 cm^{-1}). The sample was previously pressed (pressure 5 ton cm^{-2}) in the form of tablets, using KBr at amass ratio sample: KBr of 0.25 wt. %. Elemental Analyses (C, H, N) was carried out in LECO CHNS-932 (ASTM D-5373), (S) was carried out in LECOS-144DR (ASTM D-4239) and (O) was carried out in LECO VTF-900 CHNS-932 microanalysers. Both experiments, FT-IR and Elemental Analyses are important experiments to characterize all element sand bonds at adsorbent surface.

3.2.2. PURE GAS ISOTHERMS

Single gas (CO_2 and N_2) equilibrium adsorption isotherms were measured in a Magnetic Suspension Balance (MSB), by Rubotherm® (Bochum, Germany) in the pressure range of 0—10 bar at temperatures 298, 323 and 348 K. The sample was previously degassed at 423 K and 10^{-3} bar. Besides that, calibration experiments for determination of specific volumes (Vs) and volume of all components in the balance over the sample (Vb) [cm^3 g^{-1}], using He, were performed for buoyance correction. A scheme

of the mono component gas magnetic suspension balance is shown in **Figure 7**. A summary of the instrument specifications may be found in **Table 8**.

Table 8. Technical Information of the Mono Component Gas Magnetic Suspension Balance

Characteristics	**Range**
Sample Mass	0 – 25 mg
Reproducibility	±0.02 mg
Resolution	0.01 mg
Uncertain	< 0.002%
Pressure	0 – 15 MPa
Temperature	285 – 773 K

The experimental procedure to measure a single gas adsorption isotherms comprises four steps:

1. Blank Test: The main objective of this experiment is to determine port-sample volume (Vb) and mass. In this experiment, there is no adsorbent inside the nmeasument chamber and helium doses are injected in the system so as to increase pressure stepwise. Helium is as inert gas, therefore a plot of gas density [g cm^{-3}] versus mass variation [g], according to **Equation (2.14)** should give a straight line, with slope equal sample-port volume [cm^{-3}].

2. Sample Degassing: In this step, the adsorbent sample is placed in sample port and heated under vacuum (10^{-3} mbar) until 423 K, as defined from TGA characterization, for 5 hours The objective of this step is to desorb humidity and previously adsorbed gases.

3. le Specific Volume (He): After degassing, the sample specific volume (Vs) may be determined in a similar way as the blank test. Helium is injected stepwise and the slope of the plot of gas density [g cm^{-3}] versus Mass variation [g] gives the sum of specific solid volume [cm^3 g^{-1}] and Vb, according to **Equation (2.14)**.

4. Adsorption/ Desorption Isotherms: Single gas isotherms were measured by injecting the target gas in the chamber, so as to increase pressure stepwise. Mass variations were then recorded and excess adsorbed concentration can be calculated according to **Equation 2.14**. When the pressure upper limit is reached (10 bar), then pressure is decreased stepwise and the desorption branch is recorded.

Figure 7. Single Gas Magnetic Suspension Balance

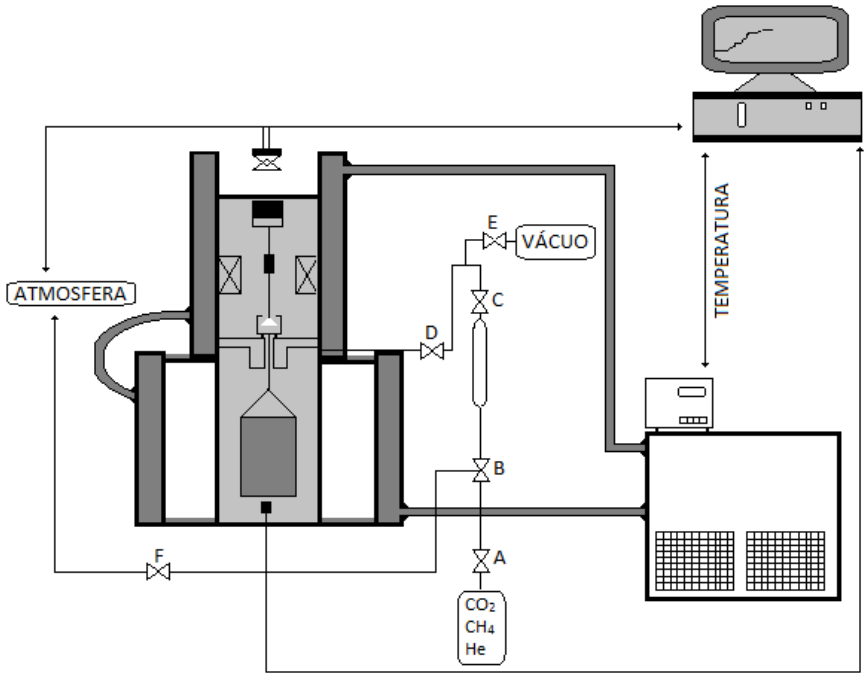

3.2.3. MIXED GASES ISOTHERMS

A multi component MSB was used to measure mixed gas adsorption equilibria. It is similar to mono component MSB in many aspects. The main difference is the dosing system to define binary composition of gases, which flow continuously through the measuring chamber. In this system, it is possible to mix gases in different compositions, so as to predict different scenarios. The main features of the instrument are summarize in **Table 9**. A schematic view of the instrument is shown in **Figure 8** (DREISBACH; STAUDT; KELLER, 1999).

Table 9. Technical Information of the Multi Component Gases MSB

Characteristics	Range
Sample Mass	0 – 25 mg
Reproducibility	±0.03 mg
Resolution	0.01 mg
Uncertain	< 0.002%
Pressure	0 – 35 MPa
Temperature	285- 673 K

The experimental procedure is similar to that of the single gas instrument, four steps are required to measure isotherms. The binary gas compositions taken into account was 12.0% CO_2 – 88.0% N_2 to mimic the relative proportion of these molecules in flue gases.

Figure 8. Mixed Gases MSB

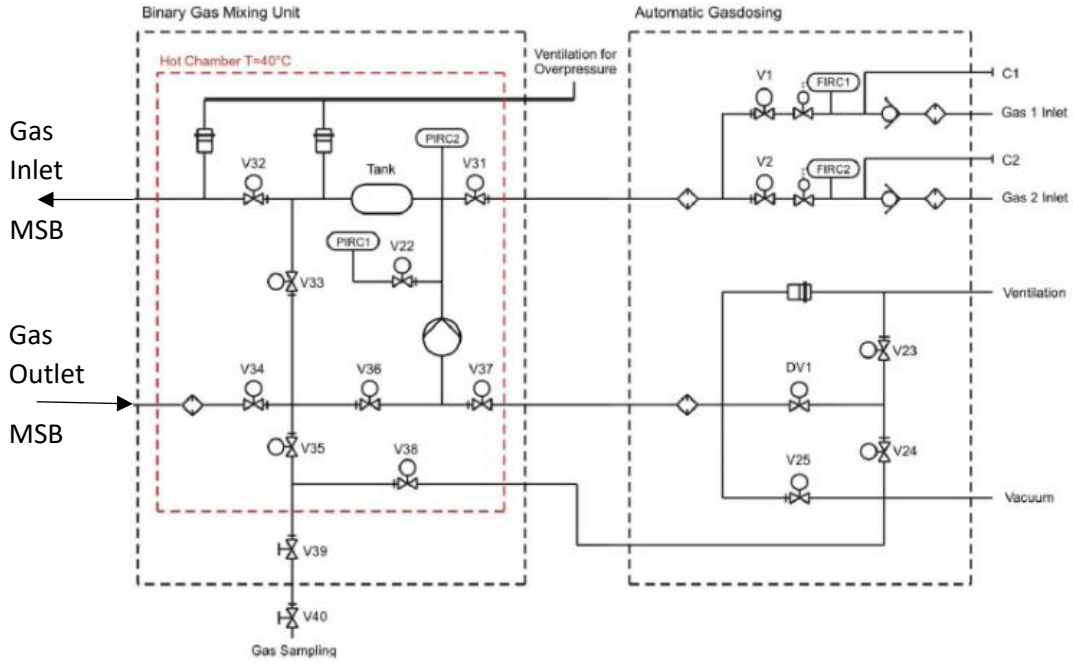

3.2.5. ADSORPTION MICROCALORIMETRY

To measure the differential enthalpy of adsorption of CO_2 as function of loading a Tian-Calvet microcalorimeter (model C80-Setaram, France) was used (**Figure 9**). It is important to note that each chamber is lined with a thermopile setup that was factory calibrated by the supplier (Setaram). The microcalorimeter was connected to an adsorption manometric setup to allow for the simultaneous measurement of the adsorption isotherm and differential enthalpy curve. All volumes in the manometric setup were previously determined by He expansion experiments.

The experimental procedure can be summarized in three steps:

1. After inserting the ACPX sample inside the measuring chamber, it was degassed (10^{-6} bar) and heated up to 423 K, for 6 h, in order to remove humidity and weakly adsorbed gases.

2. Then, a known amount of adsorbate gas is injected into the manometric setup. Pressure variations are recorded and used to calculate the adsorbed phase concentration, as in **Equation 3.1** (ROUQUEROL et al., 2014).

$$n_{ads} = \frac{P_{dos}V_{dos}}{RT_{dos}} - \frac{P_{eq}V_{total}}{RT_{eq}} \quad (3.1)$$

Where, n_{ads} is the number of moles adsorbed, P_{dos} is the injection pressure, V_{dos} is the gas volume dosed into the system, T_{dos} is the temperature of the dosed gas, R is the Ideal Gas Constant, P_{eq} is the equilibrium pressure, V_{total} is the system and injected gas volumes and T_{eq} is the equilibrium temperature. Simultaneously, the thermopile setup measures the released heat due to the adsorption process, as a calorimetric peak. The area under the peak may be converted to energy (kJ) units and then to adsorption enthalpy, as in **Equation 3.2**.

$$\Delta H_{ads\,T,n} = V_C \left(\frac{dp}{dn^{\sigma}}\right)_{T,A} + \left(\frac{dQ_{rev}}{dn^{\sigma}}\right)_{T,A} \tag{3.2}$$

Where, $\Delta H_{ads\,T,n}$ is the differential adsorption enthalpy; V_C is the dead volume of the calorimetric cell; dp is the pressure difference; dn^{σ} is the amount adsorbed given the pressure increase and dQ_{rev} is the released heat measured by the calorimeter.

3. New gas injections are performed so that gas pressure increases stepwise inside the manometric setup. For each gas injection, differential heats of adsorption and adsorbed phase concentration are calculated as in step 2; the data is treated by Calisto® Software (v1.043 AKTS-Setaram).

Figure 9. Micro Calorimetry Equipment

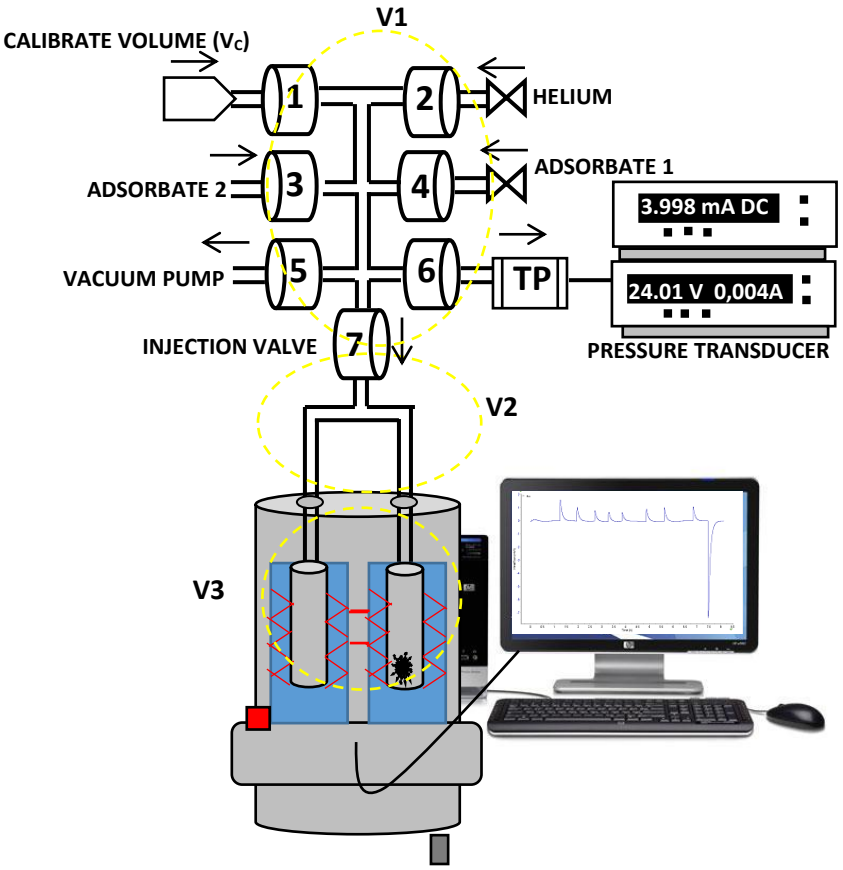

CHAPTER 4 – RESULTS AND DISCUSSION

4.1. TEXTURAL CHARACTERISTICS

The thermo-gravimetric analyses and derivate curves (TGA/DTG's) for all samples are shown in **Figure 10**. They all have a similar behavior: a mass loss event of 3-4 % until 350 K, probably due to weakly adsorbed molecules (CO_2, organics, humidity) on the surface (Sing 2014b), followed by a steady and smooth mass loss. There is a summary of all events in **Table 10**. The second mass loss rate occurs continually from 350 K to 1273 K, probably due to slow samples volatilization. By examining the derivative of the mass loss curves (blue line), it becomes clear that this first mass loss event actually comprises two peaks, at least for the samples with lowest and highest burn-offs, ACPX-22 and ACPX-76, respectively. These two peaks (labeled as 1 and 2) are apparently changing in magnitude with the increasing burn-off. Peak 1, located at approximately 323 K (**Figure 10.a**), becomes less intense as burn-off increases, whereas the opposite behavior happens to peak 2, which is located at around 412 K (**Figure 10.a**). We propose that the first peak stands for desorption of humidity and the second peak refers to desorption of atmospheric gases (such as CO_2 and organics). Based on this assumption, sample ACPX-76 would adsorb more atmospheric gases due to a supposedly higher surface area and porosity, to be confirmed by textural analysis. The least activated sample ACPX-22 would adsorb more humidity as compared to the others, either to a less hydrophobic surface or to a narrower pore size distribution, all of these to be confirmed or ruled out in the following characterization techniques. The derivative of sample ACPX-41 shows an intermediate behavior, apparently with a single peak, which may actually be the overlapping of peaks 1 and 2. Using these TGA results, a degassing temperature of 423 K for all adsorption experiments was chosen for the activated carbon samples were studied.

Figure 10. Thermo-Gravimetric Analyzes

(a) Thermo-Gravimetric Analyze for ACPX-22

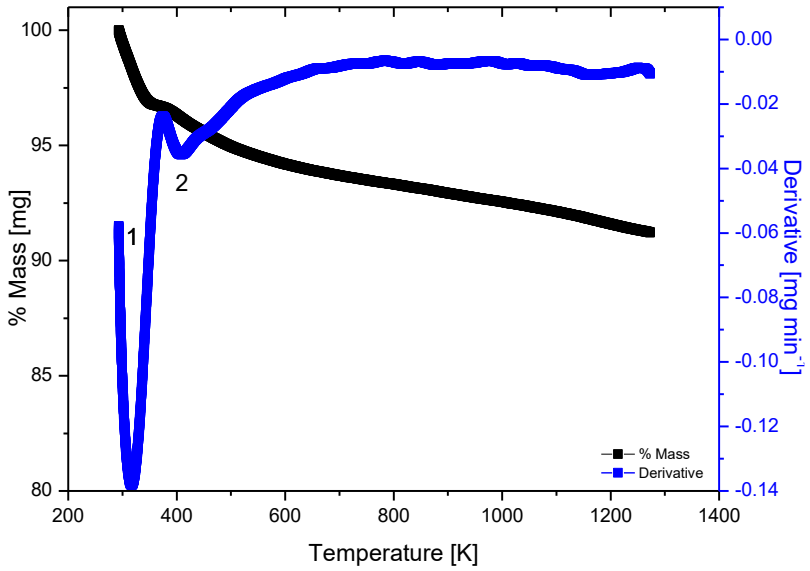

(b) Thermo-Gravimetric Analyze for ACPX-41

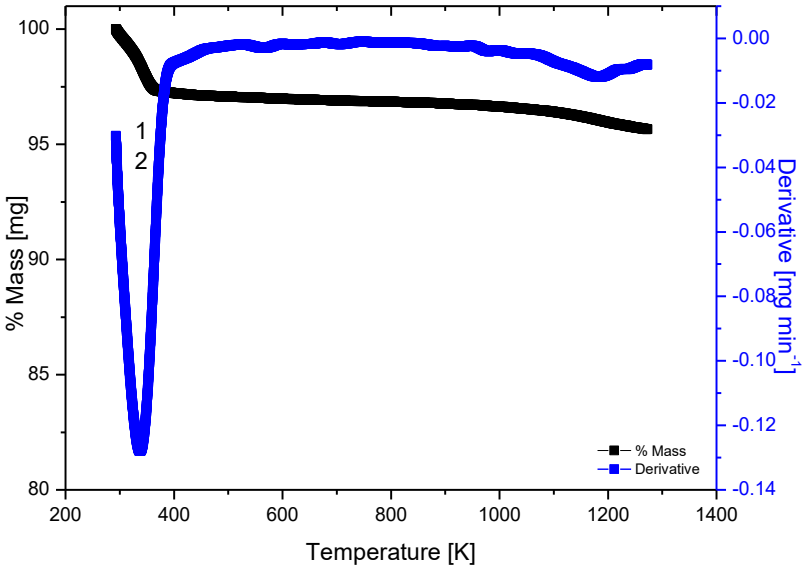

(c) Thermo-Gravimetric Analyze for ACPX-76

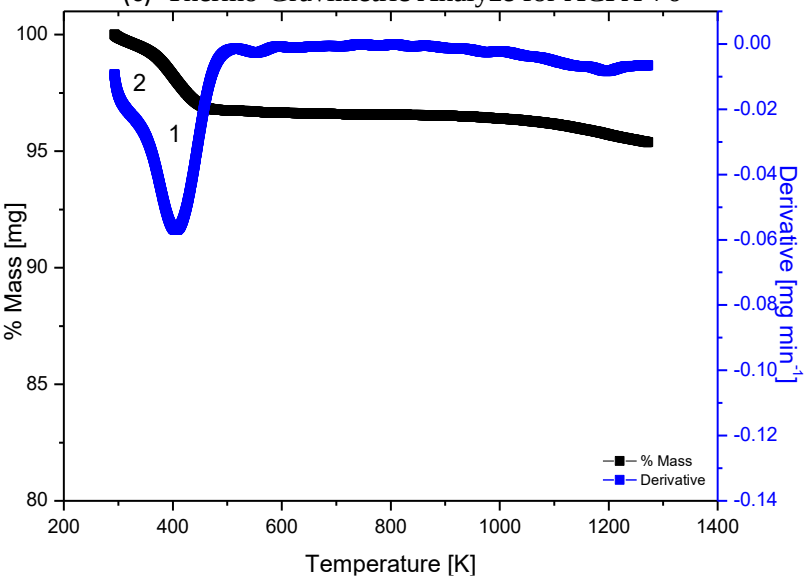

The higher temperature peak is due to the higher absolute micropore volume ratio in ACPX-76, than in the ACPX-22.

Table 10. Thermo-Gravimetric Analyzes ACPX Series

Sample	Temperature Section [K]	Average Mass Lost [%]
ACPX-22	293 – 370	4
	370 – 465	1
	465 – 1273	4
ACPX-41	293 – 360	3
	360 – 1273	2
ACPX-76	293 –351	1
	351 – 463	3
	463 – 1273	1

The elemental analysis of ACPX samples is summarized in **Table 11**. As expected from the nature of the precursor and the activation procedure, all samples are highly carbonaceous with insignificant presence of heteroatoms (N, S or O). These experiments suggest that the carbon surface is chemically homogeneous with almost no functional groups.

Table 11. Elemental Analysis

Sample	% C	% H_2	% N_2	% S	% O_2	Total
ACPX-22	95.77	0.27	0.13	0.00	0.50	96.67
ACPX-41	96.24	0.23	0.13	0.00	0.47	97.07
ACPX-76	96.90	0.23	0.13	0.00	0.51	97.77

The infrared spectra (**Figure 11**) also confirm that the samples are very homogeneous with respect to surface chemistry. The increasing burn-off (activation procedures) does not seem to affect the vibrational modes of the species present on the carbon surface. The most significant vibrational bands that could be assigned are summarized in **Table 12**. Therefore, the effect of surface chemistry on the DTG curves (**Figure 10**) is ruled out and the observed behavior can only be explained by the textural analysis.

Figure 11. Infrared Spectroscopies

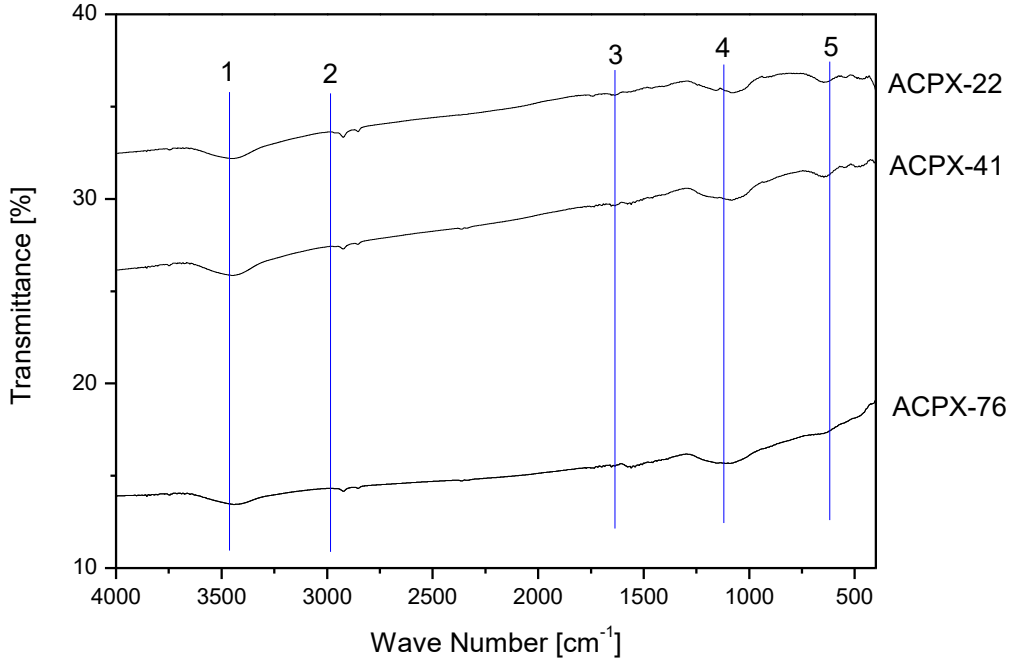

Table 12. Infrared Spectroscopies

Data Point	Wave Number Section [cm^{-1}]	Probably Link
1	3600 – 3300	H_2O; -OH
2	2950 – 2800	-CH_2; -OH; -CH; -C-C-
3	1730 – 1530	=C; -C=C-
4	1310 – 910	-CH_2; -C; -CH_3
5	730 – 430	CO_2; -CH_2

Source: Silverstein M.Robert, Webster X. Francis 2005

Nitrogen adsorption/desorption isotherms at 77K for samples ACPX-22, ACPX-41 and ACPX-76 are shown **Figure 12**. They are classified as type I (a) and (b), which are typical of microporous materials. The initial steep slope in ACPX-22 N_2 isotherm indicates a narrow distribution of micropores. Using this data, BET equation was applied in order to estimate the specific surface area. CO_2 adsorption/desorption isotherms at 273 K for all samples are also shown in (**Figure 13**). The textural properties, surface area (with the range of linearity considered in each calculation), '*C*' constant, total pore volume and micropore volume for the samples are summarized in **Table 13**. In addition, the micropore volume was also estimated from the CO_2 isotherms at 273 K.

Figure 12. Adsorption/Desorption N_2 Isotherms at 77 K

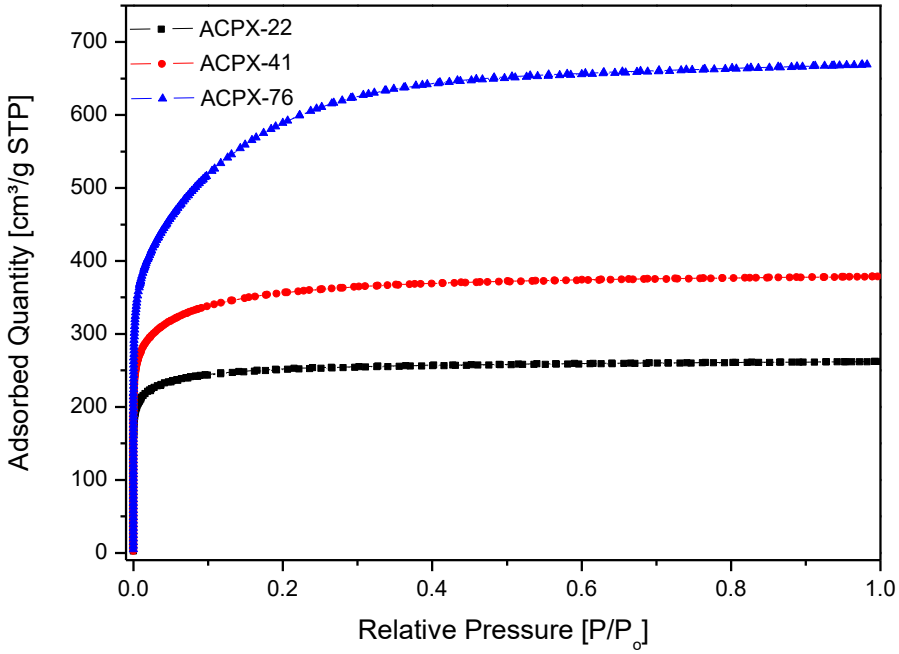

Figure 13. Adsorption/Desorption CO_2 Isotherms at 273 K

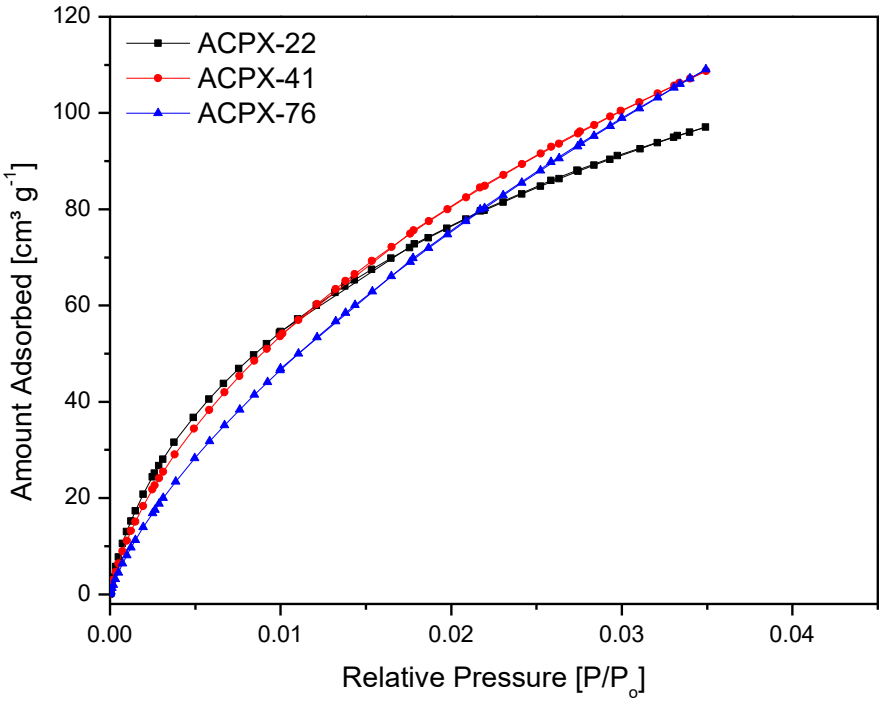

Table 13. Properties of the Obtained Activated Carbons from N_2 and CO_2 Isotherms

Sample	Surface Area BET [$m^2\ g^{-1}$]	C	Range of Linearity	Pore Volume[A] [$cm^3\ g^{-1}$]	Micropore Volume N_2[B] [$cm^3\ g^{-1}$]	Micropore Volume CO_2[B] [$cm^3\ g^{-1}$]	$\frac{Micropore}{Pore}$ [%]
ACPX-22	984	1220	0.0506 < P/Po < 0.1915	0.405	0.394	0.368	97.3
ACPX-41	1351	698	0.0504 < P/Po < 0.0758	0.585	0.500	0.522	85.5
ACPX-76	2176	126	0.0543 < P/Po < 0.1455	1.035	0.821	0.633	79.3

[A] Total pore volume, evaluated at relative pressure of 0.99
[B] Evaluated from the Dubinin-Stoeckli method

ACPX-76 has the highest N_2 uptake, around 650 $cm^3\ g^{-1}$ (**Figure 12**), due to its much higher porosity. In addition, ACPX-76 has the lowest microporosity fraction as compared to the other samples (**Table 13**). In opposition, sample ACPX-22 has the lowest total porosity, and hence the smallest N_2 uptake, around 250 $cm^3\ g^{-1}$, but the highest microporosity fraction. It is likely that such high microporosity may lead to a higher selectivity of CO_2 in gas mixtures. From data in **Table 13**, combined with isotherms in **Figure 12**, there is evidence that a higher burn-off leads to larger pore volume and wider pore size distribution, shifting towards the mesopore range. Another important remark concern the '*C*' constant values, which can be related to surface affinity towards the probe gas. Constant C increases with decreasing burn-off, which in turn is related to a narrower pore size distribution in the micropore range.

The PSD of all samples (**Figure 14**) was estimated from the N_2 adsorption isotherms by using 2D NLDFT. It is evident that an increasing the burn-off degree leads to an increase in total pore volume, so that ACPX-76 has a total pore volume 2.5 times higher that of ACPX-22. On the other hand, the longer exposure to CO_2 flux during activation also favored pore enlargement, so the PSD migrated to a wider range (larger micropores) for higher burn-off's. In addition, the PSD as given from CO_2 isotherms at 273K (**Figure 15**) was also calculated by 2D-NLDFT, allowing to zoom in the region of narrow micropores in the samples (below 1.5 nm).In **Figure 15**, PSD's as given from CO_2 isotherms are compared, up to 2 nm. The same trend as that observed for PSD's from N_2 isotherms is found. The pore size distribution shifts to wider pores as burn-off increases. Note that the peak between 0.3 and 0.4 nm, only detected in CO_2 isotherms, is observed for all samples with decreasing magnitude as burn-off increases. These ultra-micropores may be correlated to the water desorption behavior observed in TGA curves (**Figure 10**).

Figure 14. Pore Size Distributions (PSD's) by N_2 Isotherms

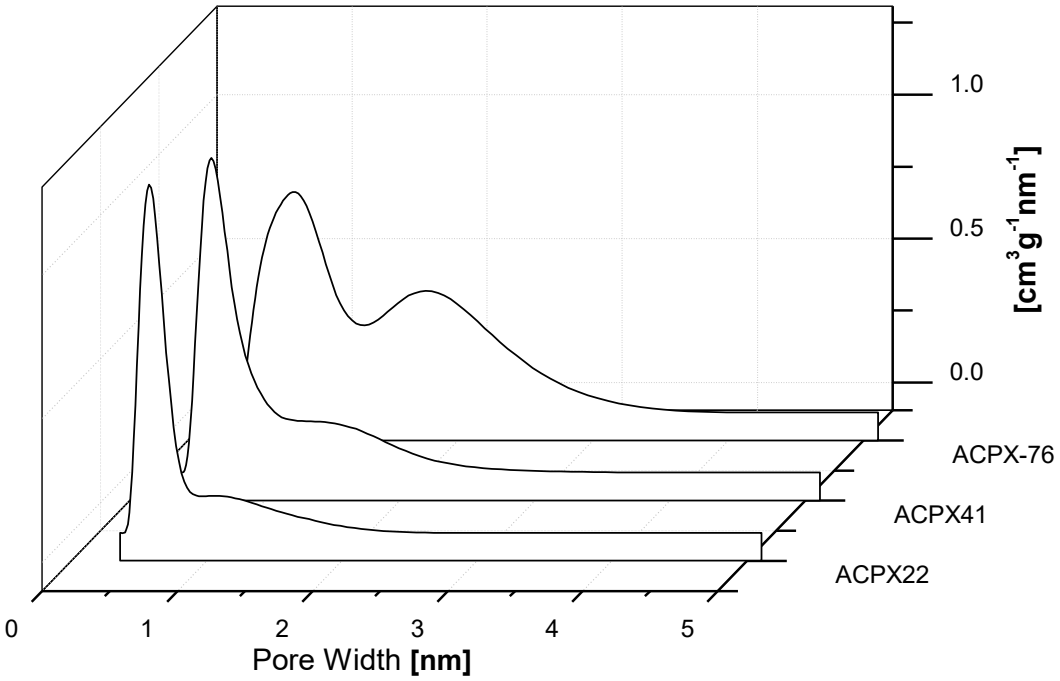

Figure 15. Pore Size Distributions (PSD's) by CO_2 Isotherms

(a) PSD by CO_2 for ACPX-22

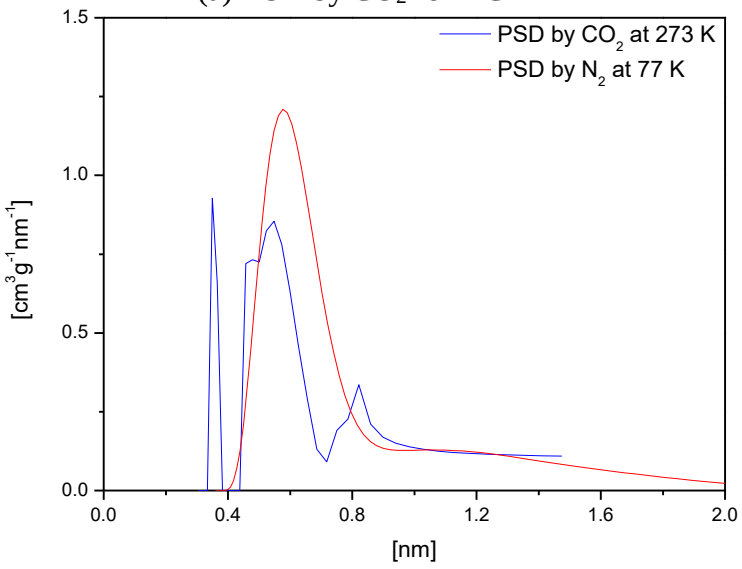

(b) PSD by CO_2 for ACPX-41

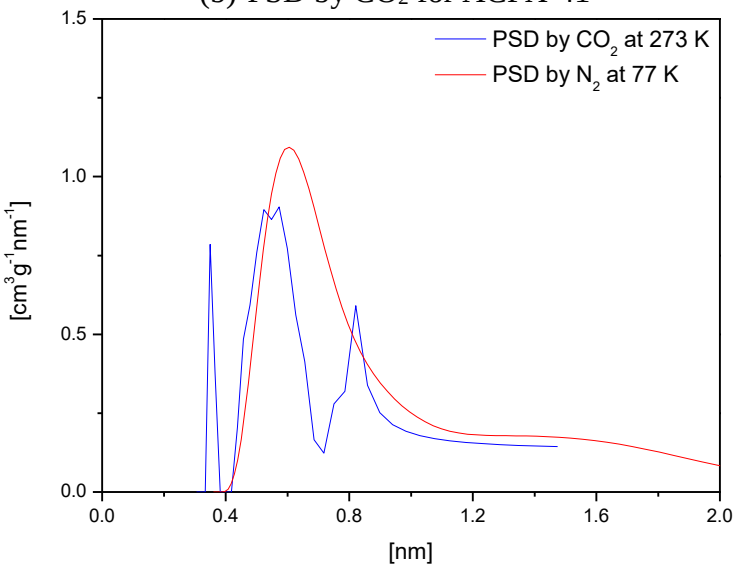

(c) PSD by CO_2 for ACPX-76

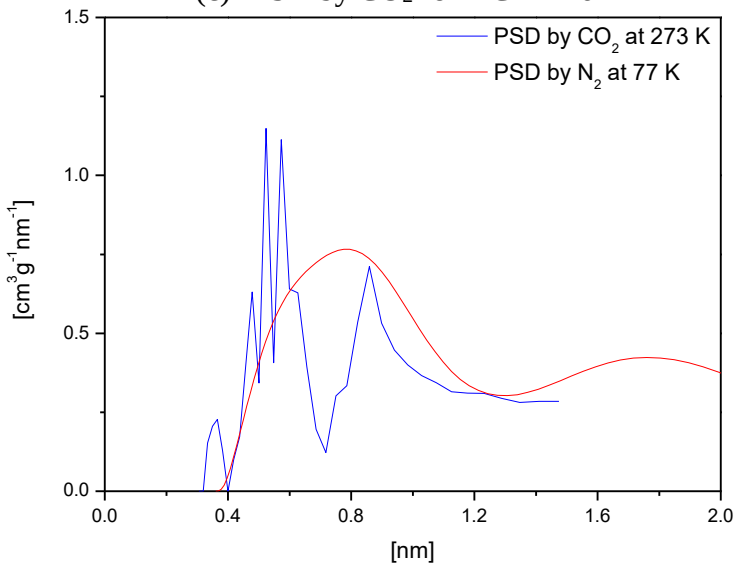

4.2. PURE GAS COMPONENT ISOTHERMS

After sample characterization as described in the previous section single component equilibrium adsorption isotherms were measured at 298, 323 and 348 K for CO_2 and N_2, which are shown in **Figures 16 (a – f)**, for all samples ACPX-22, 41 and 76. The continuous lines represent the fittings using Langmuir and Sips models. The isotherms were measured in the range from 0 to 10 bar.

Figure 16. Single Components CO_2 and N_2 Isotherms for ACPX-22, 41 and 76

(a) CO_2 Isotherms for ACPX-22

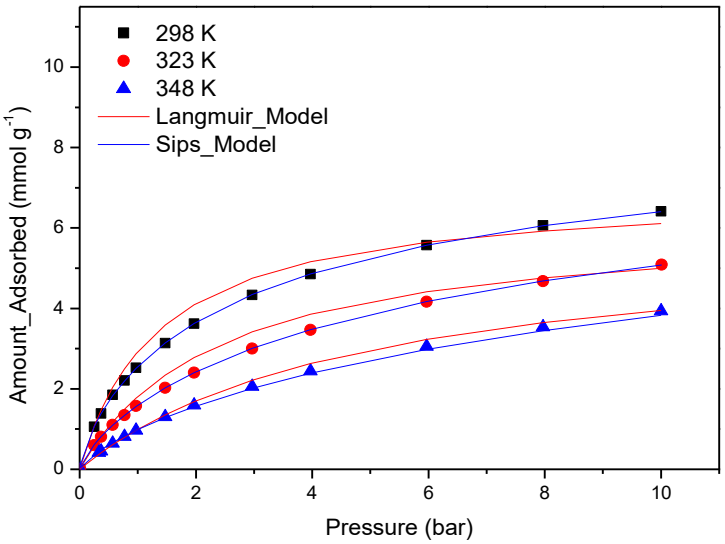

(b) N_2 Isotherms for ACPX-22

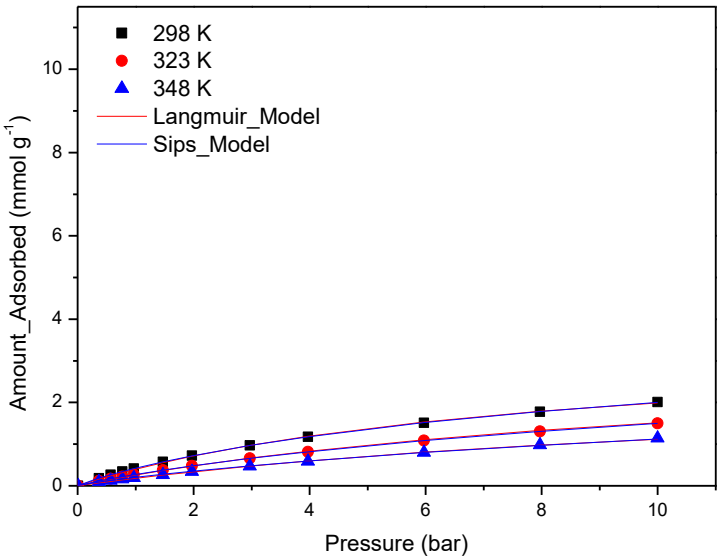

(c) CO_2 Isotherms for ACPX-41

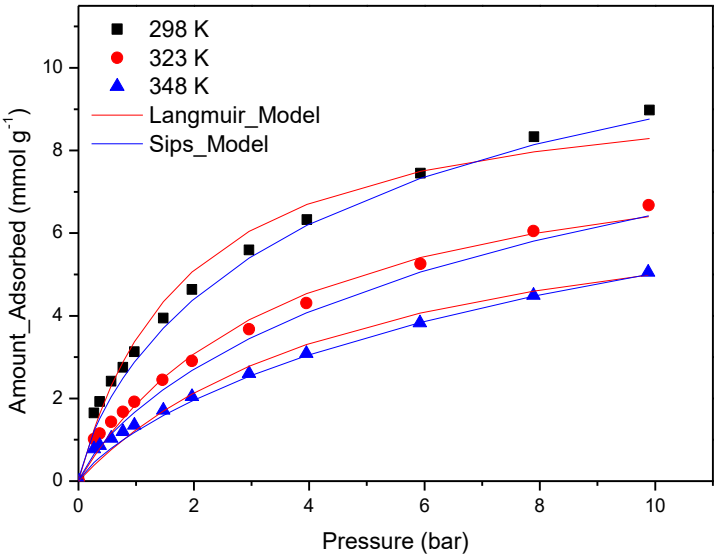

(d) N_2 Isotherms for ACPX-41

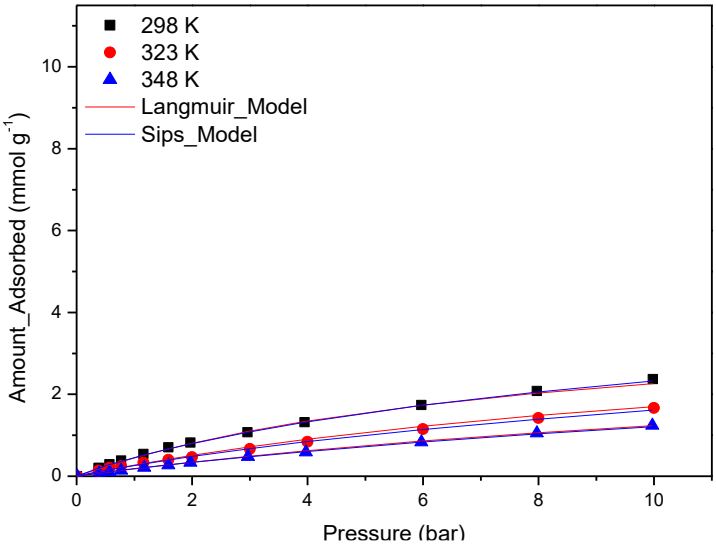

(e) CO_2 Isotherms for ACPX-76

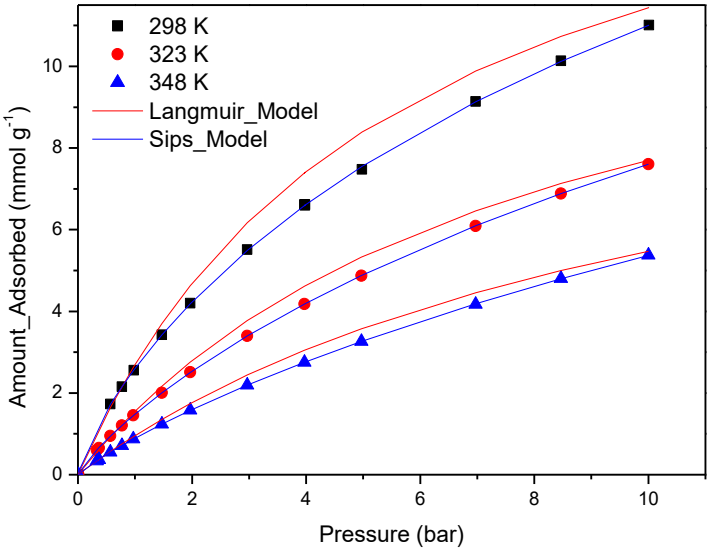

(f) N_2 Isotherms for ACPX-76

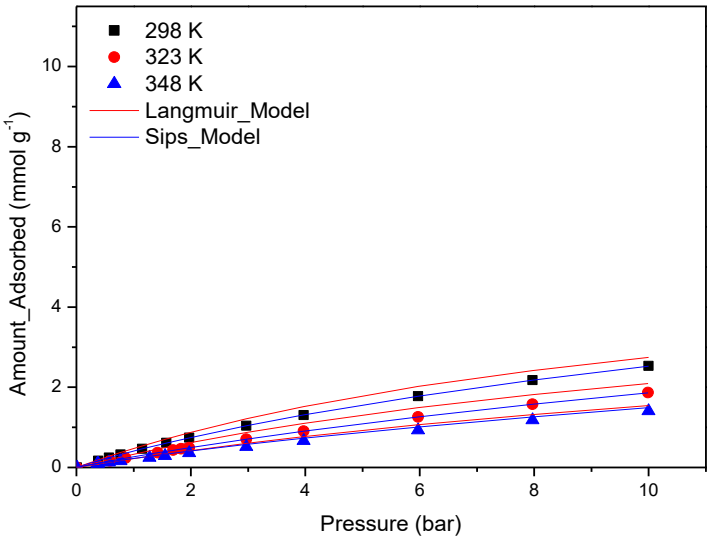

In all cases, the excess adsorbed concentration decreases with a rise in temperature, a typical behavior of physisorption. Moreover, experiments shown no hysteresis in all isotherms, which suggests full reversibility in pressure swings. CO_2 uptake is directly proportional to the burn-off, so that the more activated sample ACPX76 reaches the highest adsorbed phase concentrations. It was also observed that CO_2 uptake tends to decrease as the micropore volume decreases. This is because micropores have higher potential for physisorption, which enhance the CO_2 adsorption. It is interesting to note that the less activated the sample is, the more favorable the shape of the isotherm is, due to its narrower pore size distribution. None of the isotherms reaches a plateau in the pressure range under study because all samples have a certain degree of mesopores (sizes above 2 nm), as indicated in **Figure 14**, and they may accommodate compressed gas as pressure increases further. The adsorbent shows a higher affinity to adsorb CO_2 as compared to N_2. Some key properties of these gases, as critical temperature, molecular size and polarizability are summarized (**Table 14**).

Table 14. Adsorbates Properties

Gas	Critical Temperature [K] [1]	Molecular Size [nm] [2]	Polarizability [$\times 10^{-25}$ cm^3] [3]	Quadrupole Moment [atomic units] [4]
CO_2	304.35	0.330	29.1	2.50
N_2	126.00	0.364	17.4	1.52

Source: [4]Liu et al. 2011; [3]Rallapalli et al. 2011; [2]Pillai et al. 2008; [1]Tagliabue et al. 2009

Such properties provide explanation for the preference of the sample for CO_2. First, the diameter of CO_2 molecule is smaller than N_2 molecule, which allows for the stacking of a larger number of CO_2 molecules into the adsorbent micropores (PILLAI; PETER; JASRA, 2008; PREDESCU; TEZEL; CHOPRA, 1996). CO_2 molecule has a quadrupole

moment (Lennard-Jones potential) that induces bonding between the gas molecule and material surface (YANG, 2003). In contrast, N_2 is a weak-polar molecule, so there is no induced interaction with material surface apart from van der Waals forces. Lastly, the critical temperature decreases in the order $T_{CO2} > T_{N2}$. The high values for CO_2 critical temperature makes this gas behave like a condensable vapor at the temperature of the adsorption experiments, instead of a supercritical gas, which is the case of nitrogen.

All parameters obtained from the model fitting to mono-components isotherms and to be used for binary isotherms are summarized on **Table 15** and **Table 16**.

Table 15. CO_2 Langmuir and Sips Models Parameters

Sample			**Temperature**		
			298 K	323 K	348 K
ACPX22	Langmuir Parameters	q_{max} [g g^{-1}]	0.306	0.273	0.260
		b [bar]	0.728	0.412	0.202
	Sips Parameters	n_{max} [g g^{-1}]	0.404	0.404	0.398
		k [bar]	0.294	0.294	0.057
		C		0.777	
			298 K	323 K	348 K
ACPX41	Langmuir Parameters	q_{max} [g g^{-1}]	0.433	0.388	0.333
		b [bar]	0.536	0.268	0.196
	Sips Parameters	n_{max} [g g^{-1}]	0.640	0.600	0.540
		k [bar]	0.172	0.085	0.070
		C		0.792	
			298 K	323 K	348 K
ACPX76	Langmuir Parameters	q_{max} [g g^{-1}]	0.786	0.604	0.507
		b [bar]	0.178	0.127	0.090
	Sips Parameters	n_{max} [g g^{-1}]	1.350	1.000	0.973
		k [bar]	0.050	0.040	0.028
		C		0.838	

Table 16. N_2 Langmuir and Sips Models Parameters

Sample			**Temperature**		
			298 K	323 K	348 K
ACPX22	Langmuir Parameters	q_{max} [g g^{-1}]	0.100	0.092	0.075
		b [bar]	0.125	0.085	0.072
	Sips Parameters	n_{max} [g g^{-1}]	0.133	0.133	0.104
		k [bar]	0.074	0.074	0.039
		C		0.881	
			298 K	323 K	348 K

ACPX41	Langmuir Parameters	q_{max} [g g^{-1}]	0.115	0.115	0.102
		b [bar]	0.121	0.071	0.052
	Sips Parameters	n_{max} [g g^{-1}]	0.153	0.143	0.140
		k [bar]	0.074	0.043	0.017
		C		0.907	
			298 K	323 K	348 K
ACPX76	Langmuir Parameters	q_{max} [g g^{-1}]	0.164	0.144	0.129
		b [bar]	0.088	0.069	0.050
	Sips Parameters	n_{max} [g g^{-1}]	0.220	0.216	0.220
		k [bar]	0.045	0.030	0.020
		C		0.928	

The deviations of Langmuir and Sips fittings for all the CO_2 and N_2 mono component isotherms are shown in **Table 17** and **Table 18**. The Sips Model shows a better agreement with the experimental data, probably due to the third parameter (*C*), that is not in LM and leads to a better data mathematical fitting. Note that the parameters of the two models are coherent with their physical meaning. Parameters *b* (LM) and *k* (SM) are related to the adsorbent-adsorbate interaction. Their magnitude confirms that such interaction is stronger for the less activated sample, ACPX22, which also has the narrowest pore size distribution. Because all samples have nearly no functional groups, the different porous texture of the sample is the main feature affecting the uptake of gases and possibly the selectivity. The q_{max} parameters evidence that the maximum uptake of the samples is closely related to their total pore volume.

Table 17. Relative Squared Deviation for CO_2 Mono Components Isotherms

Sample	Model/ Temperature [K]	298 K	323 K	348 K
ACPX-22	SM	0.085	0.028	4.325
	LM	8.202	5.463	0.903
ACPX-41	SM	8.628	7.545	2.727
	LM	12.553	4.959	4.352
ACPX-76	SM	7.064	3.614	3.754
	LM	19.791	6.469	3.206

Table 18. Relative Squared Deviation for N_2 Mono Components Isotherms

Sample	Model/ Temperature [K]	298 K	323 K	348 K
ACPX-22	SM	0.061	0.001	0.010
	LM	0.036	0.022	0.030
ACPX-41	SM	0.023	0.046	3.472
	LM	0.153	0.173	0.012
ACPX-76	SM	0.009	0.079	0.029
	LM	2.143	2.207	0.610

The working capacities in the pressure interval between 1 and 4 bar are summarized in **Table 19** for all studied materials. It is important to note that, in this case, a vacuum pump would not be necessary to complete desorb the adsorbent, and pressurization up to 4 bar may be achieved with a single one-stage compressor.

Table 19. Adsorption Working Capacities (1—4 bar) for CO_2 and N_2 for ACPX-22, 41 and 76.

Gas	Temperature [K]	Working Capacity for ACPX-22 [mmol g^{-1}]	Working Capacity for ACPX-41 [mmol g^{-1}]	Working Capacity for ACPX-76 [mmol g^{-1}]
CO_2	298	2.328	3.194	4.036
	323	1.892	2.388	2.721
	348	1.473	1.735	1.876
N_2	298	0.763	0.773	0.843
	323	0.549	0.516	0.672
	348	0.395	0.374	0.499

The highest working capacities for CO_2 were obtained in ACPX-76. Further study is necessary about the selectivity and adsorption kinetics, but a higher working capacity suggests that ACPX-76 may be an interesting adsorbent for a large-scale use in cyclic process.

A comparison of ACPX-76 uptake at 4 bar and 298 K with respect to other commercial activated carbons recommended for gas adsorption and storage is shown in **Table 20**. ACPX-76 has comparable values for N_2/CO_2 selectivities, but somewhat higher capacity at those conditions.

Table 20. Activated Carbons Adsorbed Amount at 4 bar and 298 K

Activated Carbon	Adsorbed Amount [mmol g^{-1}] @ 4 bar; 298 K	
	CO_2	N_2
ACPX-22	4.85	1.18
ACPX-41	6.32	1.31
ACPX-76	6.59	1.31
WV1050[1]	4.74	0.69
Norit R1 Extra[2]	5.20	1.01
AC-1[3]	6.66	-
AC-2[3]	4.95	-

Source: [3]Kacem et al. 2015; [2]Dreisbach et al. 1999; [1]Rios et al. 2011.

4.3. BINARY GASES COMPONENTS ISOTHERMS

Adsorption isotherms for binary mixtures of CO_2 with N_2 are shown in **Figure 17. (a-c)** for ACPX-22, 41 and 76. Binary mixture mole fraction was chosen so as to be representative of a post-combustion scenario:of flue gases (12% CO_2 : 88% N_2). The points stand for experimental data and lines stand for predictions from the Extended

Langmuir (ELM), the Extended Sips (ESM) and the Multi-Region Extended Langmuir (MRELM) models using parameters obtained from single component isotherms.

Figure 17. Binary Isotherms 0.12 CO_2 and 0.88 N_2 Isotherms for ACPX-22, 60 and 76
(a) 0.12 CO_2 – 0.88 N_2 Isotherms for ACPX-22

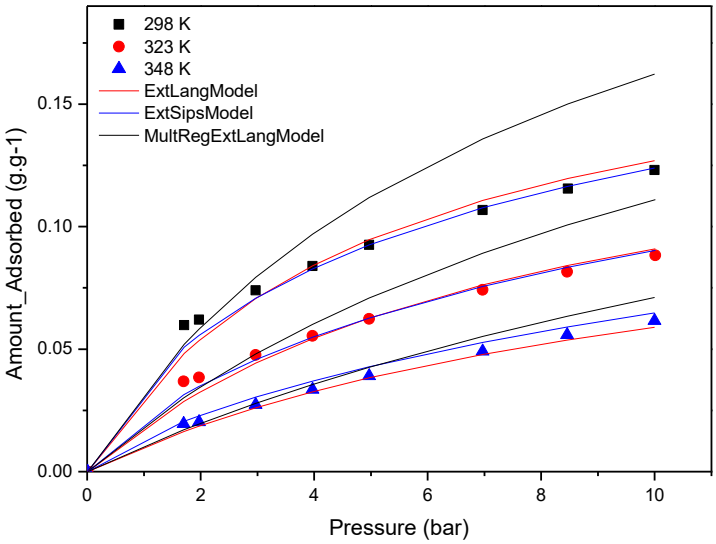

(b) 0.12 CO2 – 0.88 N2 Isotherms for ACPX-41

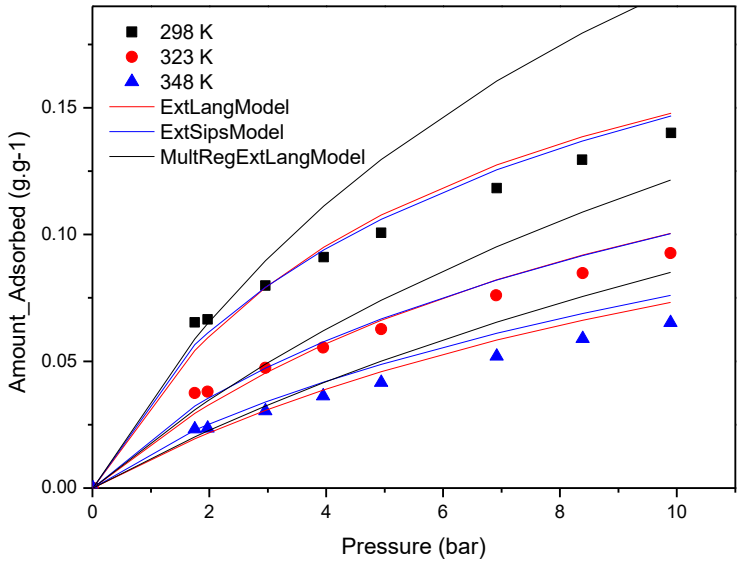

(c) 0.12 CO_2 – 0.88 N_2 Isotherms for ACPX-76

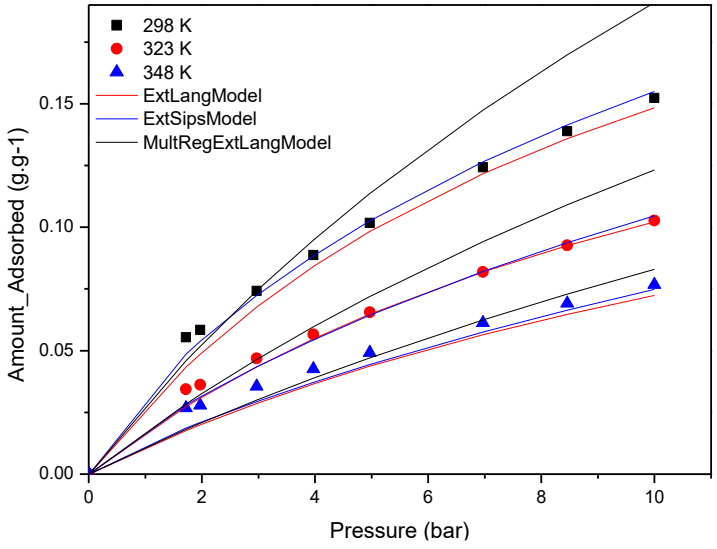

MRELM did not predict experimental data satisfactorily, especially at high pressures. The difference of this model as compared to ELM is the underlying assumption that there are adsorption sites that would only host CO_2 molecules (BAI; YANG, 2001). Indeed, this model overestimates the adsorbed phase concentration majority at high pressures. The superior prediction ability of ELM and ESM than MRELM is in agreement with the fact that ACPX family series have a homogeneous surface with no functional groups. Additionally, this information is supported by Infrared Spectroscopy experiments and Elemental Analysis. ESM had shown apparently very good fits for the single gas isotherms, which was not quite the case for binary gas data. Small deviations from single component fits may lead to significant error in binary isotherms (AHMADPOUR; WANG; DO, 1998). However, ESM and ELM showed the satisfactory prediction of experimental data of mixtures, as compared to MRELM.

The deviations of ELM, ESM and MRELM fittings for binary isotherms (0.12 CO_2; 0.88 N_2) isotherms are shown in **Table 21**. The equation of relative squared deviation was used and finally the sum of all errors in each pressure. Average deviations for all

isotherms shown equals representations for all samples using the same model. Additionally, ESM present a better adjustment with the data.

Table 21. Relative Squared Deviation for Binary Isotherms (0.12 CO_2; 0.88 N_2)

Sample	Model/ Temperature [K]	298 K	323 K	348 K
ACPX-22	ESM	2.800	1.690	2.037
	ELM	5.275	4.472	1.239
	MRELM	33.907	15.787	4.044
ACPX-41	ESM	3.658	3.209	7.253
	ELM	6.055	5.494	4.293
	MRELM	59.019	22.630	15.336
ACPX-76	ESM	1.721	3.025	9.942
	ELM	7.277	3.498	13.644
	MRELM	23.949	11.087	9.961

The measured CO_2 adsorbed phase concentrations in single gas adsorption isotherms was compared to the estimated (by ESM) adsorbed concentration in binary adsorption isotherms at the same partial pressures. These comparisons are plotted in **Figure 18. (a – c)** for all three samples. Note that, in binary isotherms, the values in the pressure axis were obtained by multiplying the total pressure in the experiment by the CO_2 mole fraction. If CO_2 completely prevented the other competing gas from being adsorbed, the pair of isotherms would overlap. Due to competition with N_2 gas, the total amount adsorbed in binary isotherms is always lower than for single CO_2 at the same pressure. This difference becomes larger at high pressures and lower temperatures.

Figure 18. CO_2 Amount Adsorbed Comparison in Single and Binary Isotherms
(a) Adsorbed CO_2 for ACPX-22

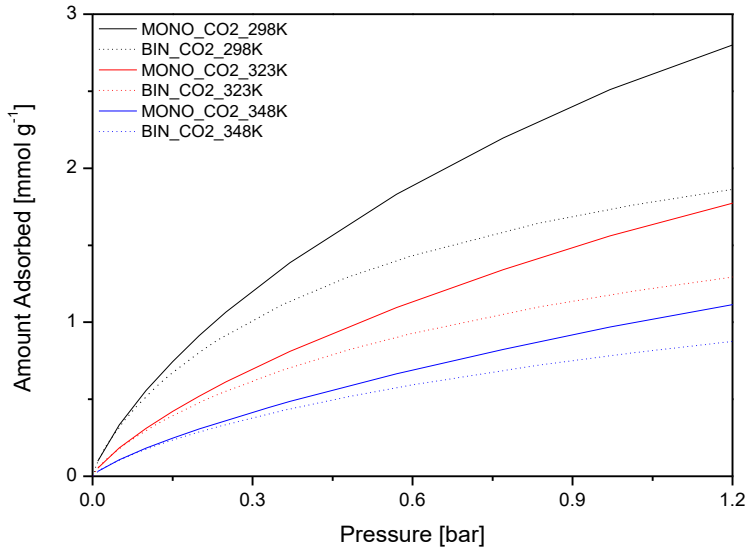

(b) Adsorbed CO_2 for ACPX-41

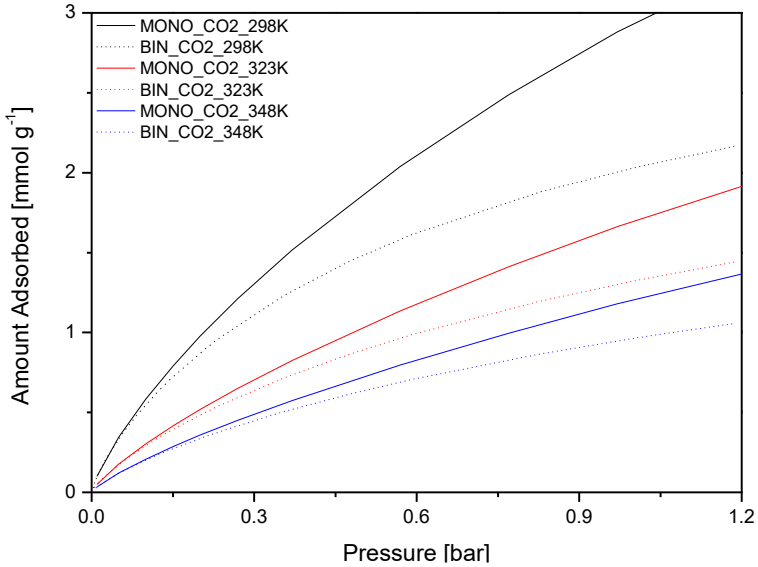

(c) Adsorbed CO_2 for ACPX-76

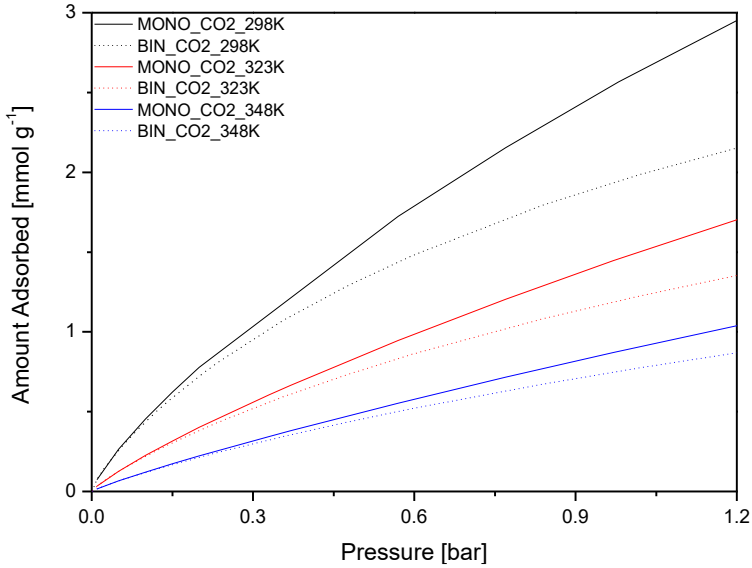

4.4. SELECTIVITY

The ACPX series selectivity were estimated from mono components isotherms (**Figure 19**) and binaries isotherms, using ESM, to obtain the CO_2 and N_2 amount adsorbed (**Figure 20**). The selectivity decreases with pressure, that means, higher selectivity values are reach at low pressures for selectivity from mono components, around 1 bar. Analyzing both results was possible perhaps that competition between gases (CO_2 and N_2) have a light negative impact in obtained selectivity values. In **Figure 19** and **20**, low pressures have a higher selectivity, because the gas molecules were not just compressed in the pores, in opposition to what occurs at high pressures. The highest values for selectivity, like expected, were obtained for ACPX-22 (22.73), than ACPX-41 (22.63) and 76 (20.25), at 298 K. in opposition to adsorption capacity, remarking this sample for next stages, like processes.

In binary isotherms, the competition effect between adsorptives causes light selectivity values reduction. In addition, the selectivity is not constant as well due to selectivity equation used from fitting isotherms with Extended Sips model. The selectivity calculated from the binary isotherms proved the enlargement pores theory in ACPX-76 occurs. The total mass amount increase, in opposition, the selectivity decreasing reduces interest in cyclic process application.

Figure 19. Selectivity from Mono Components Isotherms CO_2 and N_2

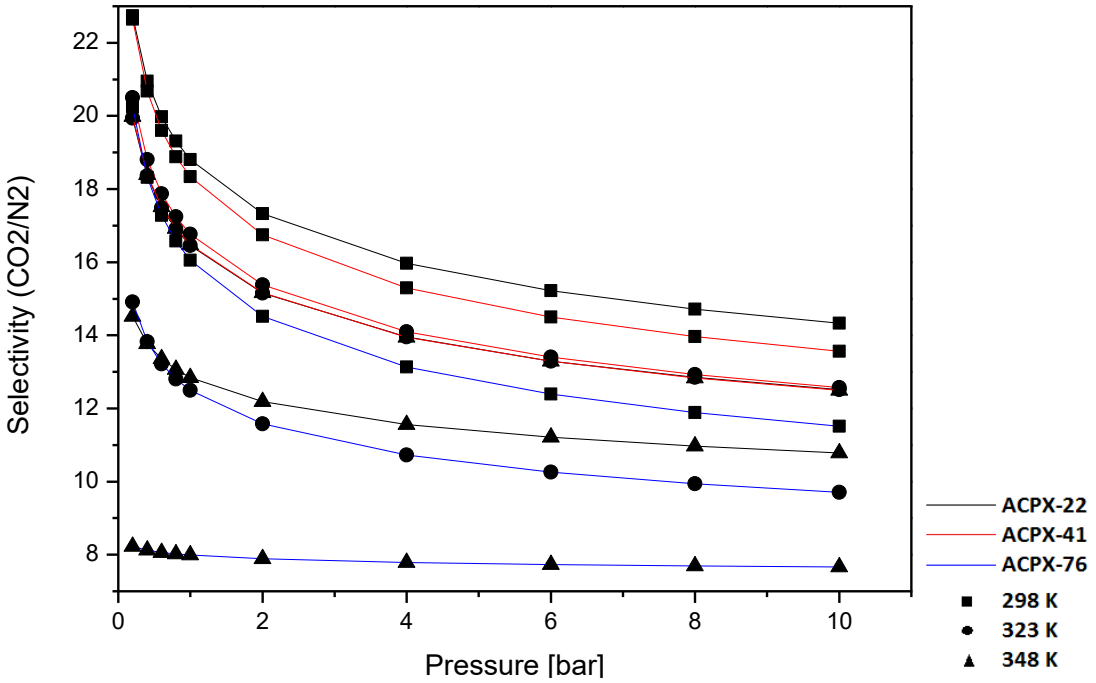

Figure 20. Selectivity from Binary Isotherms CO_2/N_2

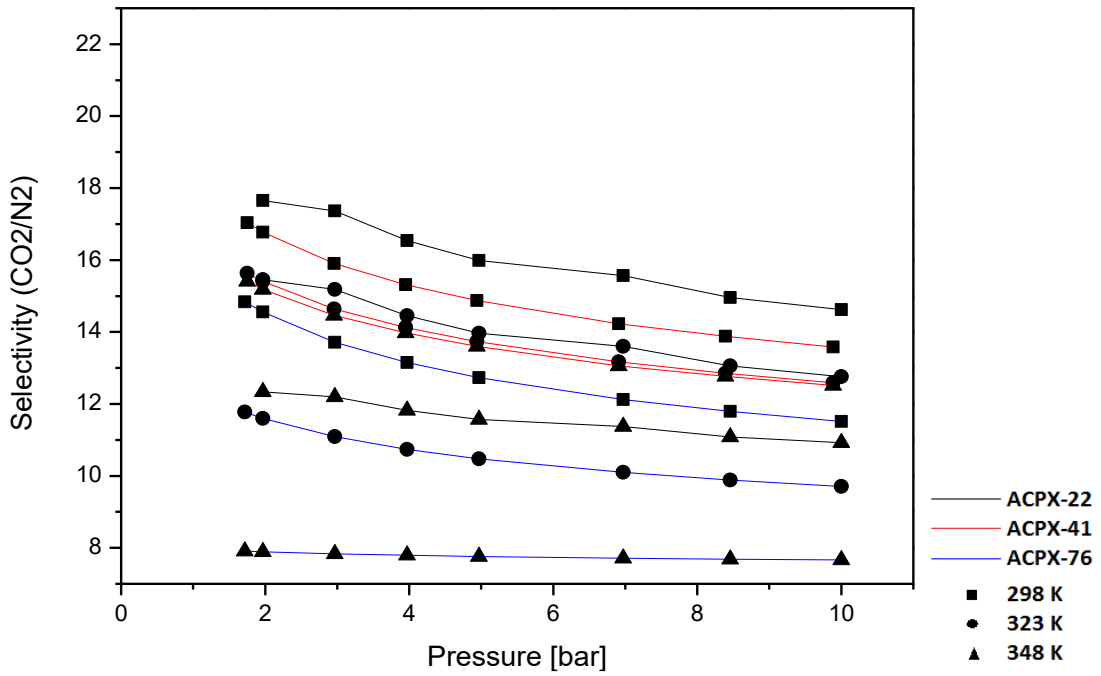

4.5. ENTHALPIES OF ADSORPTION

Experiments in a microcalorimeter were conducted for CO_2 adsorption at 298 K for the three samples and are shown in **Figure 21**. The lower energy range, below 40 kJ, obtained suggests that physisorption is the majority process in adsorption. The ACPX-76 sample has a bigger energy decrease (38.6 – 23.6 kJ mol^{-1}) with mass loading, caused by a higher proportion of different pores sizes on its structure, in the micropores range (0 – 2 nm) and in the mesopores range (2 – 50 nm). The narrower pore size distribution of the others samples, ACPX-22 and ACPX-41, lead to smaller variations in the differential adsorption enthalpy, 34.4 – 26.8 and 31.1 – 24.4 kJ mol^{-1}, respectively. Note that, above 1 mmol g^{-1} the calorimetric curves vary smoothly and their magnitude is inversely proportional to the burn-off. The average adsorption enthalpies in this range are roughly 23, 25 and 27 kJ mol^{-1} for samples ACPX-76, ACPX-41 and ACPX-22, respectively. Actually a total average values may be calculated from the total range a used for engineering purposes.

Figure 21. CO_2 Heats of Adsorption for ACPX-22, 41 and 76

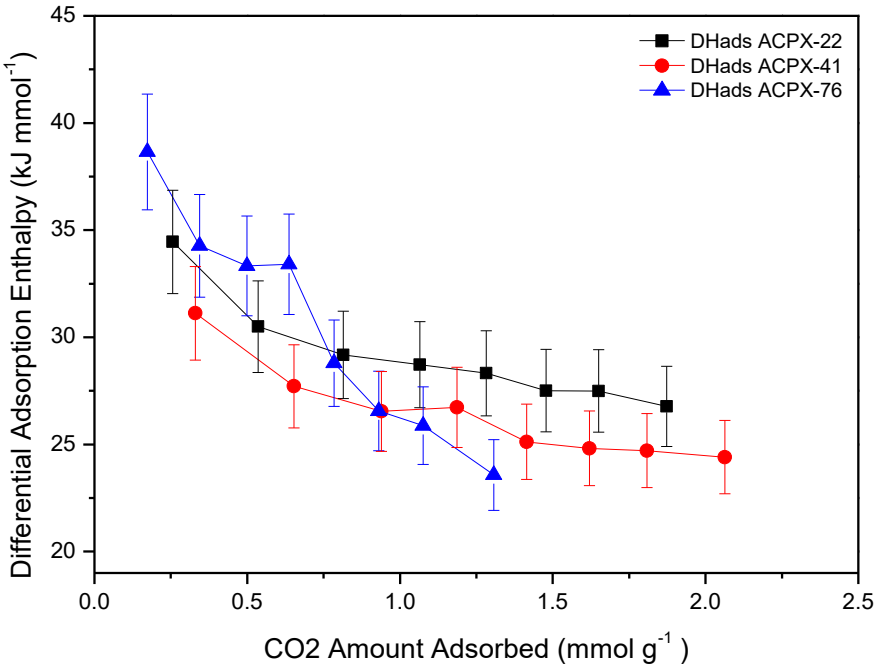

The Clausius-Clayperon equation was also applied for all samples in order to calculate the isosteric enthalpies of adsorption for CO_2 and N_2 (**Figure 22** and **23**, respectively). The isosteric enthalpies of adsorption also decrease with increasing loading; this is common behavior for microporous adsorbents (LLEWELLYN; MAURIN, 2005). In low loadings, the adsorbate chooses to sit in the most energetic adsorbent sites, then the less strong ones, which explains the shape of the curves in **Figure 22** and **Figure 23**. In the case of a homogeneous surface, small variations would be expected in the enthalpy of adsorption and this fact happens in CO_2 and N_2 adsorption. The "strength" of adsorption sites in these samples is strictly related to the relative size of pores: narrow pores provide "strong" adsorption sites and larger pores are "weaker" adsorption sites, as far as physisorption potential is concerned. Note that the utilization of Clausius-Clayperon equation is an indirect method to estimate the isosteric enthalpy of adsorption, normally used in case no experiments are not available. Comparing the enthalpy of adsorption obtained by microcalorimetry and the indirect method by Clausius-Clapeyron equation to obtain the isosteric adsorption enthalpy for CO_2 (**Figures 21** and **22**, respectively), the trends in both techniques are similar and the total enthalpy ranges agree, from 22 to 44 kJ $mmol^{-1}$. The ACPX-76 sample has the highest enthalpy variation in both cases due to its much wider pore size distribution, which provides adsorption sites with a broader range of "strength". Accordingly, ACPX-22 and ACPX-41 samples have a more discreet total enthalpy variation, due to their narrower PSD.

Figure 22. Isosteric Heats of Adsorption for CO_2 by Clausius-Clayperon Equation

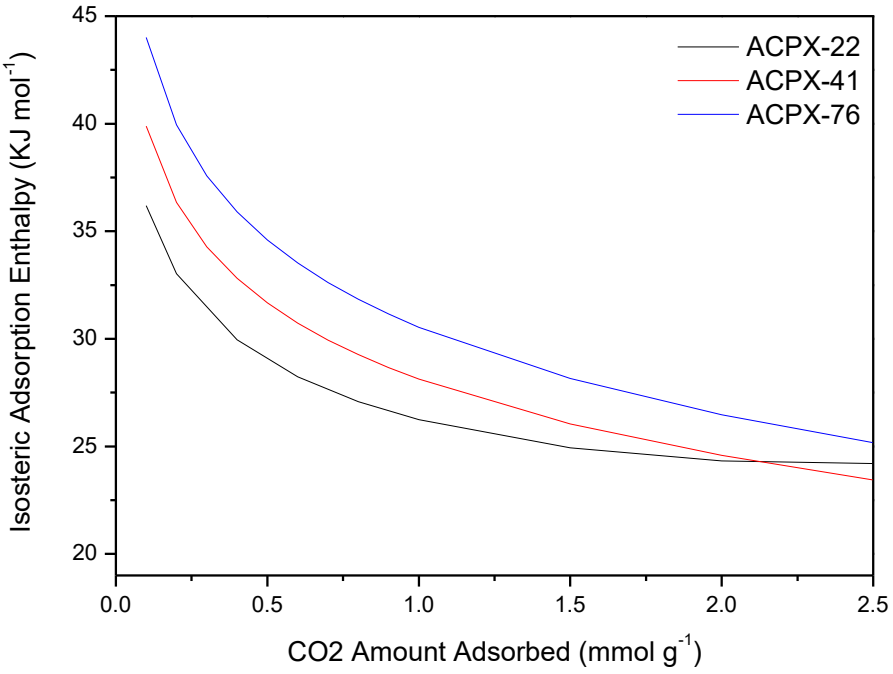

Figure 23. Isosteric Heats of Adsorption for N_2 by Clausius-Clayperon Equation

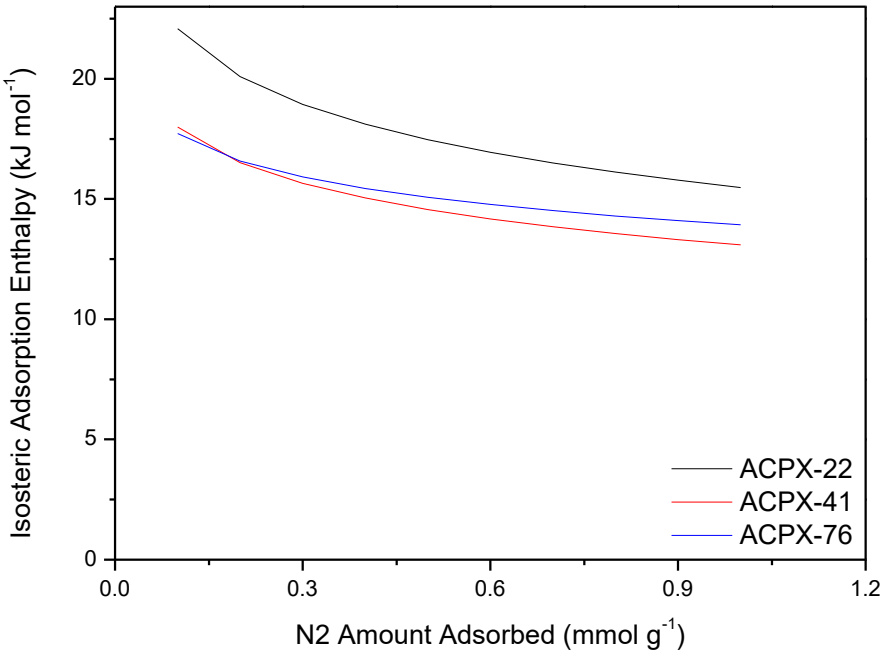

4.6. ADSORBENT PERFORMANCE INDICATOR – API

The API was calculated for a working capacity in the pressure range from 1 bar to 4 bar at 348 K (**Figure 24**). The parameters *a*, *b* and *c* were assumed as 1, following the procedure adopted to calculate the API for purification scenarios by (WIERSUM et al., 2013). The working capacity (*WC*) units have been converted to $cm^3\ cm^{-3}$ (adsorbate

volume per bed volume). This is a more physically meaningful parameter from an industrial point of view because the adsorbent will pack columns which occupy a given volume (footprint). To convert the adsorbed concentration to volume units the Ideal Gas Law was used (**Equation 4.1**). To convert the adsorbent mass to volume, a packing density of 0.3 g cm^{-3} was assumed. The packing density was roughly measured in the laboratory, by weighing the mass of adsorbent that can fill a given volume in a graduated cylinder. The average adsorbent enthalpy was 27, 25 and 23 kJ mol^{-1} for ACPX-22, 41 and 76 respectively, as explained previously.

$$\rho = \frac{P \cdot MM}{R \cdot T} \tag{4.1}$$

Where, *P* is the gas pressure, *MM* is the gas molar mass, *R* is the Gas Ideal Constant and *T* is the gas temperature.

In **Figure 24**, the ACPX-41 sample has the highest API (1.60), due to its high selectivity in this scenario, the others variables (working capacity and adsorption enthalpy) reaching intermediate values. Samples ACPX-22 and ACPX-76 have practically the same API, due to their intermediate selectivity and low adsorption enthalpy. By way of comparison, the API at 298, 323 and 348 K was calculated (**Table 22**), it is possible to note that API is very affected by temperature, because most of this variables change with temperature, as working capacity and selectivity.

Figure 24. API for ACPX-22, 41 and 76 at 348 K

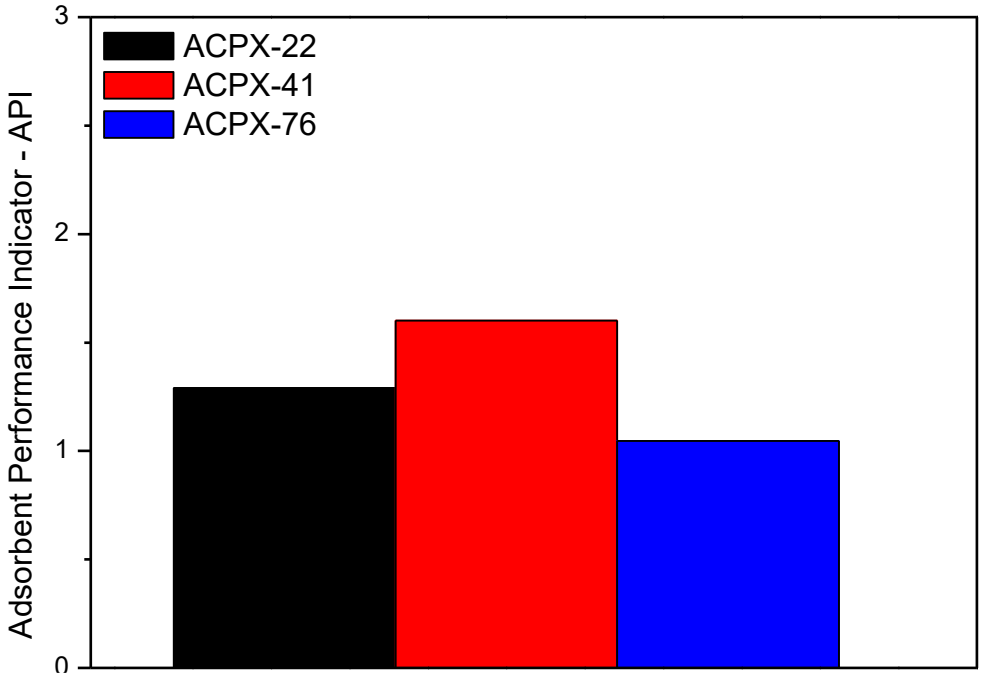

Table 22. API and Variables at 298, 323 and 348 K

Sample	Temperature [K]	Working Capacity 1 – 4 bar [$cm^3\ cm^{-3}$]	Selectivity CO_2/N_2	Adsorption Enthalpy [$kJ\ mol^{-1}$]	API
ACPX-22	298	15.04	15.88	29.11	7.68
	323	5.19	13.87		2.29
	348	3.57	11.51		1.29
ACPX-41	298	21.46	15.20	26.39	11.55
	323	5.25	14.02		2.59
	348	3.28	13.87		11.60
ACPX-76	298	27.12	13.05	30.55	10.70
	323	5.93	10.67		1.88
	348	4.71	7.78		1.05

CHAPTER 5 – CONCLUSION

Activated carbons samples prepared by physical activation of PET wastes led to adsorbents with a very hydrophobic surface (no functional groups) and an interesting porous texture for gas adsorption purposes. Total pore volume and surface area increased in the following order in the ascending order of burn-off degree: ACPX-22< ACPX-41 < ACPX-76, with pore sizes in the range from 0.3 to 2 nm. The fraction of micropores with respect to the total pores decreases with increasing burn-off: 97.3, 85.5, 79.3 % for samples ACPX-22, ACPX-41 and ACPX-76, respectively. Higher burn-off leads to pore enlargement, which in turn causes a reduction in the selectivity of CO_2 with respect to N_2. Comparisons between CO_2 mono component isotherms and CO_2/N_2 binary isotherms shown that all samples experience a similar decrease in adsorption capacity of CO_2, due to N_2 competition. The estimated selectivity from mono component and binary isotherms, as expected, are higher for samples with a narrower PSD and vary as follows: ACPX-22 (22.73), ACPX-41 (22.63) and ACPX-76 (20.25). Despite these differences brought about by different burn-off degrees, the degassing temperature of all samples was not appreciably affected (423 K), which ensures complete desorption of humidity and atmospheric gases). ACPX-76 has the highest working capacity (1.876 mmol g^{-1}) in the range from 1 to 4 bar at all temperatures under study (298 K, 323 K and 348 K). The differential adsorption enthalpy vary in the range from 23 to 44 kJ mol^{-1} and are coherent with the respective PSD.

Sample ACPX-76 would seem superior for CO_2 capture as compared to the other samples, due to its much higher working capacity at all temperatures under study. Nevertheless, at typical temperatures of flue gas emissions (348 K), the superiority of ACPX-76 is overcast by a much lower selectivity towards N_2. Sample ACPX-41 turns out to have more interesting properties to cyclic separation processes, as indicated by the performance indicator, API. It also has an intermediate burn-off (41 %) and adsorption enthalpy, so that its final price may be inferior to that of ACPX-76 and costs associated with adsorbent regeneration may be lower than that of ACPX-22.

CHAPTER 6 – SUGGESTIONS FOR FUTURE WORK

Taking into consideration its application in real processes, the study of the kinetics is necessary to account for diffusion mechanisms and aid the simulation of the performance of pressure-swing cyclic process. The next stages of this research should include experiments and simulations on a fixed bed setup, where hydrodynamic, heat and mass transfer aspects come into play. With the knowledge of thermodynamic and transport phenomena in the particle level (subject of this thesis) and column level, simulations of a cyclic process (like PSA or VSA) may be performed to check for performance parameters (purity, recovery, energy consumption, adsorbent productivity) to calculate capture costs.

Another path to be followed is the study of these samples for CH_4 or natural gas storage and transport, given their extremely developed porosity in the micropore range. Previous studies showed that this class of materials (activated carbons from PET, activated with CO_2 flow) have a high affinity to adsorb CH_4 as well. Research about the adsorption equilibrium and kinetics for this application is strongly advised.

REFERENCES

AHMADPOUR, A.; WANG, K.; DO, D. D. Comparison of models on the prediction of binary equilibrium data of activated carbons. **AIChE Journal**, v. 44, n. 3, p. 740–752, 1998.

ALBANEZ, Nelma Elisa Farias Kunrath. **Preparação E Caracterização De Nanocompósitos Preparados Com Argilas Amido E Sacarose**. 2008. 91 f. PhD thesis in Materials and Metalurgic Engineering - São Paulo University [s.l: s.n.].

BAE, Y. et al. Separation of CO 2 from CH 4 Using Mixed-Ligand Metal - Organic Frameworks. **Langmuir**, n. 18, p. 8592–8598, 2008.

BAI, R.; YANG, R. T. A Thermodynamically Consistent Langmuir Model for Mixed Gas Adsorption. **Journal of colloid and interface science**, v. 239, n. 2, p. 296–302, 2001.

BLAZSÓ, M. Recent trends in analytical and applied pyrolysis of polymers. **Journal of Analytical and Applied Pyrolysis**, v. 39, n. 1, p. 1–25, jan. 1997.

BRUNAUER, S. et al. On a Theory of the van der Waals Adsorption of Gases. **J. Am. Chem. Soc.**, v. 62, n. 7, p. 1723–1732, 1940.

BUNN, R. DE P. D. C. W. B. The Crystal Structure of Polyethylene Terephthalate. **Royal Society of London A, Mathematical and Physical Sciences**, p. 531-542, 1954.

BUTLER, James H., MONTZKA, Stephen A. THE NOAA ANNUAL GREENHOUSE GAS INDEX (AGGI). United States, 2014. Available in: <http://www.esrl.noaa.gov/gmd/aggi/aggi.html>. Accessed at: 12/21/2015.

DE STEFANI, V.; BABA-AHMED, A.; RICHON, D. Experimental determination of carbon dioxide and nitrous oxide co-solubility in liquid oxygen. **Fluid Phase Equilibria**, v. 207, n. 1–2, p. 131–142, 2003.

DI BERNARDO, Luiz. **Métodos e técnicas de tratamento de água**. 2 ed. Campo Grande, 2005.

DREISBACH, F.; STAUDT, R.; KELLER, J. U. High pressure adsorption data of methane, nitrogen, carbon dioxide and their binary and ternary mixtures on activated carbon. **Adsorption**, v. 5, n. 3, p. 215–227, 1999.

DUBININ, M. M.; STOECKLI, H. F. Homogeneous and heterogeneous micropore structures in carbonaceous adsorbents. **Journal of Colloid And Interface Science**, v. 75, n. 1, p. 34–42, 1980.

DUNNE, J. A. et al. Calorimetric Heats of Adsorption and Adsorption Isotherms. 1. O 2 , N 2 , Ar, CO 2 , CH 4 , C 2 H 6 , and SF 6 on Silicalite. **Langmuir**, v. 12, n. 24, p. 5888–5895, jan. 1996.

ENERGY TOMORROW. **Natural Gas**. Available in: <http://naturalgas.org/overview/background/>. Accessed at: 12/21/2015.

ESSENHIGH, R. H. Potential Dependence of Global Warming on the Residence Time (RT) in the Atmosphere of Anthropogenically Sourced Carbon Dioxide. **Energy & Fuels**, v. 23, n. 5, p. 2773–2784, 21 maio 2009.

FIGUEROA, J. D. et al. Advances in CO2 capture technology-The U.S. Department of

Energy's Carbon Sequestration Program. **International Journal of Greenhouse Gas Control**, v. 2, n. 1, p. 9–20, 2008.

GARCIA, S. et al. Predicting mixed-gas adsorption equilibria on activated carbon for precombustion CO2 capture. **Langmuir**, v. 29, n. 20, p. 6042–6052, 2013.

GARG, A.; SHUKLA, P. R. Coal and energy security for India: Role of carbon dioxide (CO2) capture and storage (CCS). **Energy**, v. 34, n. 8, p. 1032–1041, 2009.

IPCC. **Summary for policymakers, in: climate change 2014, mitigation of climate change. contribution of working group III to the fifth assessment report of the intergovernmental panel on climate change**. New York, 2014.

JAGIELLO, J. et al. Dual gas analysis of microporous carbons using 2D-NLDFT heterogeneous surface model and combined adsorption data of N2 and CO2. **Carbon**, v. 91, p. 330–337, set. 2015.

KACEM, M.; PELLERANO, M.; DELEBARRE, A. Pressure swing adsorption for CO 2 / N 2 and CO 2 / CH 4 separation : Comparison between activated carbons and zeolites performances. **Fuel Processing Technology**, v. 138, p. 271–283, 2015.

KANNICHE, M. et al. Pre-combustion, post-combustion and oxy-combustion in thermal power plant for CO2 capture. **Applied Thermal Engineering**, v. 30, n. 1, p. 53–62, 2010.

KIM, J.; KANG, B. DBPs removal in GAC filter-adsorber. **Water Research**, v. 42, n. 1–2, p. 145–152, 2008.

KIM, Y. E. et al. Comparison of carbon dioxide absorption in aqueous MEA, DEA, TEA, and AMP solutions. **Bulletin of the Korean Chemical Society**, v. 34, n. 3, p. 783–787, 2013.

KOROS, W. J.; FLEMING, G. K. Membrane-based gas separation. **Journal of Membrane Science**, v. 83, n. 1, p. 1–80, 1993.

KRUPA, S. V; KICKERT, R. N. The Greenhouse effect: impacts of ultraviolet-B (UV-B) radiation, carbon dioxide (CO2), and ozone (O3) on vegetation. **Environmental pollution (Barking, Essex : 1987)**, v. 61, n. 4, p. 263–393, 1989.

LANGMUIR, I. The Adsorption of Gases on Plane Surfaces of Glass, Mica and Platinum. **Journal of the American Chemical Society**, v. 40, n. 9, p. 1361–1403, 1918.

LIU, J. et al. Molecular Simulations and Theoretical Predictions for Adsorption and Diffusion of CH 4 / H 2 and CO 2 / CH 4 Mixtures in ZIFs. **The Journal of physical chemistry C**, v. 115, p. 12560–12566, 2011.

LLEWELLYN, Phillip. **Recent Advances in Gas Separation by Microporous Ceramic Membranes**: Characterisation of microporous materials by adsorption microcalorimetry, v. 6, Amsterdam, The Netherlands, Elsevier Masson SAS, 2000.

LLEWELLYN, P. L.; MAURIN, G. Gas adsorption microcalorimetry and modelling to characterise zeolites and related materials. **Comptes Rendus Chimie**, v. 8, n. 3–4, p. 283–302, 2005.

MARKET, R. China Activated Carbon Industry Report , 2014-2017. p. 5441, 2017.

MURATA, K.; KANEKO, K. The General Equation of Supercritical Gas Adsorption Isotherm. **The Journal of Physical Chemistry B**, v. 105, n. 36, p. 8498–8503, 2001.

MYERS, A L.; PRAUSNITZ, J. M. Thermodynamics of mixed-gas adsorption. **AIChE Journal**, v. 11, n. 1, p. 121–127, jan. 1965.

PARRA, J. et al. Textural characterisation of activated carbons obtained from poly(ethylene terephthalate) by carbon dioxide activation. In: **Studies in Surface Science and …**. [s.l.] Elsevier Masson SAS, 2002. v. 144p. 537–543.

PARRA, J. et al. Structural Changes in Polyethylene Terephthalate (PET) Waste Materials Caused by Pyrolysis and CO 2 Activation. **Adsorption Science & Technology**, v. 24, n. 5, p. 439–449, jun. 2006.

PARRA, J. B. et al. Textural development and hydrogen adsorption of carbon materials from PET waste. **Journal of Alloys and Compounds**, v. 379, n. 1–2, p. 280–289, out. 2004a.

PARRA, J. B. et al. High value carbon materials from PET recycling. **Applied Surface Science**, v. 238, n. 1–4, p. 304–308, nov. 2004b.

PILLAI, R. S.; PETER, S. A.; JASRA, R. V. Adsorption of carbon dioxide, methane, nitrogen, oxygen and argon in NaETS-4. **Microporous and Mesoporous Materials**, v. 113, n. 1–3, p. 268–276, 2008.

PLASTICS EUROPE. **Plastics – the Facts 2016**. Belgium, 2016.

PRAETORIUS, B.; SCHUMACHER, K. Greenhouse gas mitigation in a carbon constrained world: The role of carbon capture and storage. **Energy Policy**, v. 37, n. 12, p. 5081–5093, 2009.

PREDESCU, L.; TEZEL, F. H.; CHOPRA, S. Adsorption of nitrogen, methane, carbon monoxide, and their binary mixtures on aluminophosphate molecular sieves. **Adsorption**, v. 3, n. 1, p. 7–25, 1996.

QUIRKE, N.; TENNISON, S. R. R. The interpretation of pore size distributions of microporous carbons. **Carbon**, v. 34, n. 10, p. 1281–1286, 1996.

Whinfield, John R. Polymeric Linear Terephthalic Esters. **United States Patent Office**, 1949.

RIOS, R. B. et al. Experimental analysis of the efficiency on charge/discharge cycles in natural gas storage by adsorption. **Fuel**, v. 90, n. 1, p. 113–119, jan. 2011.

RITTER, J.A., EBNER, A. D. State-of-the-art Adsorption and Membrane Separation Processes for Carbon Dioxide Production from Carbon Dioxide Emitting Industries. **Journal of Chemical Information and Modeling**, v. 44, p. 1273–1421, 2009.

RODRIGUEZ-REINOSO, F., LINARES-SOLANO, A. **Chemistry and Physics of carbono**. New York: [s.n.], 1988, Volume 21 ed.

ROUQUEROL, Françoise, et al. **Adsorption by Powders and Porous Solids**, 2 ed. France, Elsevier, 2014.

RUTHVEN, Douglas. **Principles of Adsorption and Adsorption Properties**. New York: A Wiley-Interscience publication, 1984.

SANDRU, M.; HAUKEBØ, S. H.; HÄGG, M.-B. Composite hollow fiber membranes for CO2 capture. **Journal of Membrane Science**, v. 346, n. 1, p. 172–186, 2010.

SERREZE, M. C. Understanding recent climate change. **Conservation biology : the**

journal of the Society for Conservation Biology, v. 24, n. 1, p. 10–17, 2010.

SHEKHAWAT, Dushyant. A review of carbon dioxide selective membranes : A topological report. **United States Department of Energy**, 93 f, 2003.

SILVERSTEIN M. Robert, WEBSTER X. Francis, Kiemle J. David. **Spectrometric Identification of Organic Compounds**. United States: John Wiley & Sons, 2005.

SILVESTRE-ALBERO, J. et al. Physical characterization of activated carbons with narrow microporosity by nitrogen (77.4 K), carbon dioxide (273 K) and argon (87.3 K) adsorption in combination with immersion calorimetry. **Carbon**, v. 50, n. 9, p. 3128–3133, 2012.

SING, K. S. W. et al. International union of pure and applied chemistry(IUPAC). **Pure Appl. Chem.**, v. 57, p. 603–619, 1985.

SING, K. S. W. et al. Assessment of Mesoporosity. In: **Adsorption by Powders and Porous Solids**. [s.l.] Elsevier, 2014. v. 270p. 269–302.

SING, K. S. W. Assessment of Surface Area by Gas Adsorption. In: **Adsorption by Powders and Porous Solids**. 2. ed. [s.l.] Elsevier, 2014. p. 237–268.

SING, K. S. W.; ROUQUEROL, F.; ROUQUEROL, J. Classical Interpretation of Physisorption Isotherms at the Gas–Solid Interface. In: **Adsorption by Powders and Porous Solids**. [s.l.] Elsevier, 2014. p. 159–189.

TAGLIABUE, M. et al. Natural gas treating by selective adsorption: Material science and chemical engineering interplay. **Chemical Engineering Journal**, v. 155, n. 3, p. 553–566, 2009.

THITAKAMOL, B.; VEAWAB, A. Foaming model for CO2 absorption process using aqueous monoethanolamine solutions. **Colloids and Surfaces A: Physicochemical and Engineering Aspects**, v. 349, n. 1–3, p. 125–136, 2009.

THOMMES, M. et al. Physisorption of gases, with special reference to the evaluation of surface area and pore size distribution (IUPAC Technical Report). **Pure and Applied Chemistry**, v. 87, n. 9–10, p. 1051–1069, 1 jan. 2015.

TÓTH, József. **Adsorption : theory, modeling, and analysis**. New York: Marcel Dekker, 2001.

TÓTH, J. On thermodynamical inconsistency of isotherm equations: Gibbs's thermodynamics. **Journal of Colloid and Interface Science**, v. 262, n. 1, p. 25–31, 2003.

TUINIER, M. J. et al. Cryogenic CO2 capture using dynamically operated packed beds. **Chemical Engineering Science**, v. 65, n. 1, p. 114–119, 2010.

VASEGHI, M. R.; AMIRI, A.; PESARAN, A. A review of energy efficiency and CO<inf>2</inf> emissions in the US cement industry. **2012 IEEE-IAS/PCA 54th Cement Industry Technical Conference**, p. 1–9, 2012.

VILARRASA-GARCÍA, E. et al. CO2/CH4 adsorption separation process using pore expanded mesoporous silicas functionalizated by APTES grafting. **Adsorption**, v. 21, n. 8, p. 565–575, 2015.

WADSÖ, I. Isothermal microcalorimetry near ambient temperature: An overview and discussion. **Thermochimica Acta**, v. 294, n. 1, p. 1–11, 1997.

WIERSUM, A. D. et al. An adsorbent performance indicator as a first step evaluation of novel sorbents for gas separations: Application to metal-organic frameworks. **Langmuir**, v. 29, n. 10, p. 3301–3309, 2013.

WONG, S.; BIOLETTI, R. Carbon dioxide separation technologies. **Alberta Research Council**, 2002.

YANG, Hongqun, et al. Progress in carbon dioxide seperation and capture: A review. Journal of Enviromental Science, v. 20, p. 14–27, 2008.

YANG, T. Ralph. **Adsorbents Adsorbents : Fundamentals and Applications**. United States: John Wiley & Sons, 2003.